THESIS FOR THE DEGREE OF LICENTIATE OF ENGINEERING

Advances in the application of an early and selective recovery of lithium from spent lithium-ion batteries via hydrometallurgical methods

Léa M.J. ROUQUETTE

Industrial Material Recycling

Department of Chemistry and Chemical Engineering

CHALMERS UNIVERSITY OF TECHNOLOGY

Gothenburg, Sweden 2023

Advances in the application of an early and selective recovery of lithium from spent lithium-ion batteries via hydrometallurgical methods

Léa M.J. ROUQUETTE

Technical report no 2023:04

Department of Chemistry and Chemical Engineering
Industrial Material Recycling
Chalmers University of Technology
SE-412 96 Gothenburg
Sweden
Telephone + 46 (0)70-264-2796

Printed by Chalmers digitaldryck
Gothenburg, Sweden 2023

Advances in the application of an early and selective recovery of lithium from spent lithium-ion batteries via hydrometallurgical methods

Léa M.J. Rouquette
Industrial Material Recycling
Department of Chemistry and Chemical Engineering
Chalmers University of Technology

Abstract

In 2020 alone, the use of electric vehicles (EVs) contributed to more than 50 Mt CO_2-eq of savings in GHG emissions globally. Given their performance in terms of energy and power density, Lithium-ion batteries (LiBs) are the technology of choice for the success of rapid EV growth. The demand for elements such as cobalt, nickel, copper, and lithium has increased widely. The concern regarding the availability of lithium is growing, and countries are rushing to establish policies to ensure a stable supply of critical minerals for EV battery supply chains. Lithium was added to a list of critical raw materials in 2020, and new regulations are pushing towards the recycling of more materials. The recovery target for lithium is set at 70% by 2030.

Current recycling systems do not have a high lithium recovery rate. Pyrometallurgy does not allow its recycling, while the current hydrometallurgy processes exhibit lithium losses. Traditional flowcharts are very complex. Usually disregarded, there has not been a major push to develop a recycling process centred around lithium. New recycling strategies are trying to lift its importance by recovering lithium in the first step. Early selective and more efficient recovery of lithium from spent lithium-ion batteries is the main objective of the research. The focus of this study was the investigation of early and complete lithium recovery. Two promising methods are considered: a combination of a thermal treatment followed by water leaching and a full hydrometallurgical route involving the use of oxalic acid as a leaching agent. The experiments were carried out using real LiB waste.

The use of thermal treatment on spent batteries presents many advantages. It allows for safer handling of the battery cell and the reduction of waste volume. Moreover, the metal oxides undergo a reduction forming more leachable species. At the same time, the reaction between lithium dioxide and carbon dioxide form lithium carbonate, a water-soluble species. The highest lithium recovery (62%) is achieved after pyrolysis at 700°C for 1h and water leaching at 25°C for 1h with a solid-to-liquid ratio of 20 g/L. Aluminium is the only co-dissolved element. On the other hand, the use of oxalic acid led to a 98.8% leaching yield for lithium, while less than 0.5 % of cobalt and nickel, and 1.5% of manganese were leached when applying leaching at 60°C, 1h, 0.6 M oxalic acid. Moreover, aluminium is completely leached, which is one of the novel findings in this field. Nickel, cobalt, and manganese oxalates are insoluble and remain in the solid residue, while lithium oxalate is dissolved in the solution.

Keywords: Lithium, recycling, hydrometallurgy, thermal treatment, organic acid.

List of Publications and Manuscripts

This thesis is based on the following paper and manuscript:

Paper I

Léa MJ ROUQUETTE, Tom LEMAÎTRE, Nathália VIECELI, Martina PETRANIKOVA. Intensification of lithium carbonation in the thermal treatment of spent EV Li-ion batteries via waste utilization and selective recovery by water leaching. Resources, Conservation & Recycling Advances, 2023, vol. 17, p. 200125. https://doi.org/10.1016/j.rcradv.2022.200125

Contribution: Main author and most experimental work and analysis of data.

Manuscript II

Léa M.J. Rouquette, Martina Petranikova, Nathália Vieceli. Complete and Selective recovery of lithium from EV lithium-ion batteries: modelling and optimization using oxalic acid as a leaching agent.

Submitted to Separation and Purification Technology
Contribution: Main author and all experimental work and analysis of data.

Table of contents

1 INTRODUCTION 1

1.1 GOAL AND DRIVING FORCES 2

2 BACKGROUND 3

2.1 LITHIUM-ION BATTERY 3

2.2 CURRENT RECYCLING PROCESSES 4

2.3 STATE-OF-THE-ART IN EARLY RECOVERY OF LITHIUM FROM LIBS 7

3 THEORY 11

3.1 CARBOTHERMIC REDUCTION DURING THE THERMAL TREATMENT 11

3.2 LEACHING 13

4 MATERIALS AND METHODS 15

4.1 BLACK MASS 15

4.2 CHEMICALS 15

4.3 EQUIPMENT 16

4.4 DESIGN OF EXPERIMENTS 18

5 EXPERIMENTAL PROCEDURE 21

5.1 APPROACH 1 (PAPER I) 21

5.2 APPROACH 2 (PAPER II) 22

6 RESULTS AND DISCUSSIONS 23

6.1 APPROACH 1 23

6.2 APPROACH 2 29

7 SUMMARY AND CONCLUSIONS 39

8 FUTURE WORK 41

ACKNOWLEDGMENTS 43

BIBLIOGRAPHY 45

Abbreviations and definitions

The following abbreviations and definitions are used throughout this thesis:

%P	Leachate purity
%Y	Leaching yield, percentage extracted
ΔG	Gibbs Free Energy (in kJ)
BEV	Battery electric vehicle
CO_2	Carbon Dioxide
DTG	Differentiate Thermogravimetric
EPR	Extended producer responsibility
EU	European Union
EV	Electric vehicle
F^-	Fluorine
FTIR	Fourier-Transform Infrared Spectroscopy
g	Gram
GHG	Greenhouse gases
GWh	Gigawatt-hours
H_2O	Water
HF	Hydrogen Fluoride
ICP-OES	Inductively Coupled Plasma - Optical Emission Spectrometry
IEA	International Energy Agency
kJ	Energy in kilo joules
L	Litre
LCE	Lithium carbonate
LFP	Lithium Iron Phosphate cathode material
LH	Lithium hydroxide
Li_2O	Lithium oxide
LiB	Lithium-Ion Battery
LiF	Lithium Fluoride
$LIPF_6$	Lithium Hexafluorophosphate
mg	Milligram
ml	Millilitre
N_2	Nitrogen
NCA	Nickel Cobalt aluminium oxide cathode material
NMC	Lithium Nickel Manganese Cobalt Oxide
ºC	Degree Celsius
PE	Polyethylene
PHEV	Plug-in Hybrid vehicle
PP	Polypropylene
rpm	Rotation per minute
S/L	Solid to liquid ratios
t	tonnes
USGS	United State Geological Survey
vol%	Volume percent
wt%	Weight Percentage
XRD	X-Ray Diffraction

1 Introduction

Transport is one of the major contributors of greenhouses gases (GHG). In fact, it accounted for 37% of CO_2 emissions from end-use sectors in 2021 [1], which represents around 15% of global GHG emissions. In 2020 alone, the use of electric vehicles (EVs) contributed to more than 50 Mt CO_2-eq of savings in GHG emissions globally [2]. To support and enhance the deployment of this technology, policies, and targets have been legislated by governments all around the world [3]. For example, the EU announced that by 2035, only zero-emission vehicles will be sold within its borders [4]. Hence, the global sales of electric vehicles (all modes; plug-in hybrid vehicles (PHEV) and battery electric vehicles (BEV)) have been rising strongly for the last decade. An 75% increase in sales was observed between 2021 and 2022 [3]. Given their performance in terms of energy and power density, lithium-ion batteries (LiBs) are the technology of choice for the success of rapid EV growth [5,6].

LiBs currently consume about 74% of the total lithium production [3,7]. Global lithium consumption was projected to be about 41.5 kt in 2017 [8], while it was estimated at 93 kt in 2021 [9]. The International Energy Agency (IEA) has evaluated future demand based on 3 different policy scenarios [3]:

1) In the Stated Policies Scenario, annual lithium demand would reach about 330 kt by 2030, a fourfold increase relative to 2021.
2) In the Announced Pledges Scenario, annual lithium demand would reach 500 kt, a sixfold increase.
3) In the Net Zero emissions scenario, an outrageous amount is estimated: about 750 kt in 2030.

Lithium can be found in four types of deposits, primarily in brines and hard rocks (mostly pegmatite rock) but also in sedimentary rocks and seawater [10]. Approximately 78% of the global lithium resources are found in the brines. These salt lakes are mainly located in South America [11]. USGS' Mineral Commodity Summaries 2022 reports that global lithium resources total 89 million metric tons, and the estimated reserve of lithium is about 22 million metric tons (about 25% of the total resources) [9]. Lithium production increased by 21% in 2021, with the main producing countries being Australia, Argentina, Chile, and China [9]. The EU share of the world reserves is only 1%, with only 0.4% of the global primary production coming from Portugal in 2019 [12]. Hence, the EU's reliance on lithium is estimated at 100%, meaning that Europe is entirely dependent on the rest of the world for lithium-processed material. Moreover, the price rose from USD 7,000 per ton of lithium carbonate equivalent (LCE) to USD 26,000 in November [9].

Considering the availability of lithium and growing demand and price, countries are rushing to establish policies to ensure a stable supply of critical minerals for EV battery supply chains. The European Commission established a list of critical raw materials based on the economic importance and supply risk of each material. This initiative gives better guidance and framework for the European strategy. It will also help research and innovation to focus on the critical elements [13]. Lithium was added to the list in 2020. The Battery Directive (2006/66/EC) and the Waste Electrical and Electronic Equipment (WEEE) Directive (2012/19/EU) regulate and give a legal framework for the management of batteries, and a new regulation proposal in 2020 requests

the re-enforcement of these legislations. One implementing act consists of establishing a battery passport for each industrial and EV battery placed on the market. This should allow economic operators to more efficiently gather and reuse the information and develop an appropriate framework to deploy the collection of each battery [14]. Focus is placed on the end of life of such waste, establishing recycling as a necessary tool in waste management. The new target for LiB recycling efficiency is 70% by 2030. Zooming in on the materials, 95% of the cobalt, nickel, and copper are expected to be recovered along with 70% of the lithium [14]. Moreover, the implementation of a percentage requirement for recycled material in newly produced batteries is pushing toward better recycling processes. In numbers, new LiBs are expected to contain 12% recycled cobalt, 6% recycled lithium, and 4 % recycled nickel [14].

The recycling of spent LiBs is indeed an obligation for multi-dimensional benefits such as keeping all the valuable metals in one place, reusing those metals during the manufacturing process, decreasing battery production costs, having a better environmental policy, saving natural resources, protecting the future, and conserving resources for future generations [15]. The EU, a big battery consumer, will have an increasing waste stock in upcoming years. Processing the waste will become more profitable. The Global Electric Vehicle Outlook 2022 reports that the recycling rate for lithium is lower than 1% [3,12] and the official end-of-life recycling input in the EU is 0% [12].

Pyrometallurgy and hydrometallurgy methods can be used to process spent LiBs and recover the valuables elements. However, the current recycling systems do not achieve a high recovery rate for lithium. No lithium is recovered at all using pyrometallurgy methods, while hydrometallurgy methods suffer losses at each step, leading to a decrease in the total recovery. Lithium is probably the most critical material for EVs, followed very closely by the supply of nickel and cobalt. Until recently, the price of cobalt was one of the main incentives for recycling. The increase in lithium price serves as a motivator for recyclers to aim for its recovery. Moreover, the production of lithium battery-grade products is challenging, as it requires very high purity, over 99.9%.

1.1 Goal and driving forces

The goal of this research is to increase the total lithium recovery. With that aim, the working direction is to develop a new, robust, and sustainable process for the recycling of LiBs, in which lithium is recovered as the first step of the process, through the use of greener chemicals. Two main routes are investigated: a combination of pyro and hydrometallurgy and a pure hydrometallurgical process. Both are very promising and could lead to increased lithium recovery. Some specification of these methods is needed to improve and understand the process.

Approach 1 is a thermal treatment of the black mass followed by selective water leaching. Lithium carbonate can be recovered after evaporative crystallization. Approach 2 consists of the oxalic acid leaching of the black mass. In this work, all the major elements present in the waste will be tracked to know their behaviour in the process. This is very important, as some impurities such as aluminium and fluoride, are challenging to handle, since they have a strong affinity with lithium.

2 Background

2.1 Lithium-ion battery

As mentioned in the introduction, given their performance in terms of energy and power density, LiBs are the technology of choice for the success of rapid EV growth [5,6]. Due to its properties, lithium is an ideal candidate for batteries, and so far, very few commercial lithium-free alternative batteries exist on the market with the same type of properties. The substitution of lithium is not expected at a large scale in the upcoming years. Nevertheless, we can mention that sodium-ion batteries are gaining increased attention [3], as a potential alternative to LiBs. Moreover, next-generation batteries, such as solid-state batteries, still require lithium in their products. The research is ongoing, and there could be many breakthroughs in the future.

There are three main categories of cathode materials that are relevant nowadays: nickel-based chemistry batteries, comprising NMC ($LiNi_xM_yCo_zO_2$, Lithium Nickel-Manganese-Cobalt Oxide) and NCA ($LiNi_{0.8}Co_{0.15}Al_{0.05}O_2$, Lithium Nickel-Cobalt-Aluminium Oxide), LCO ($LiCoO_2$, Lithium Cobalt Oxide), and LFP ($LiFePO_4$, Lithium Iron Phosphate). NMC chemistry is currently the most popular technology used in EVs [16]. However, a resurgence of LFP has been observed in the market.

An NMC positive electrode is composed of lithium nickel-manganese-cobalt oxide. Their molar ratios can vary from one battery to another. The ratio is indicated in the name, i.e., NMC111 or NMC 811. The oxide particles are mixed with a polymer binder (polyvinylidene fluoride, PVDF) and coated onto an aluminium foil that acts as a current collector. The negative electrode is generally a graphite layer coated on a copper foil with the same binder polymer. The electrolyte in between is normally a mixture of one or more dipolar organic solvents and a lithium salt, such as lithium hexafluorophosphate ($LiPF_6$). A porous polymeric membrane usually made of polypropylene (PP) or polyethylene (PE) acts as a separator and prevents short circuits, thereby ensuring cell safety [17]. The movement of the lithium ions from the positive to negative side provokes the movement of electrons generating the energy. A battery cell is composed of a certain number of successive layers of anode and cathode immersed in the electrolyte. The battery cells are then assembled in battery packs that make up the battery module used in EVs. The casing is usually made of steel, aluminium, and plastic.

The average composition by weight for each component of the battery cells is presented in Figure 1. The cathode active material occupies 15–40 wt% of the battery cell. The elemental composition varies depending on the chemistry, but an estimation range is as followed: 3–20 wt% cobalt, 2–15 wt% nickel, 2–7 wt% lithium, and 2–10 wt% manganese [18,19]. The binder is present in a range of 1–4 wt%, and fluoride and phosphorous content is rarely given [19].

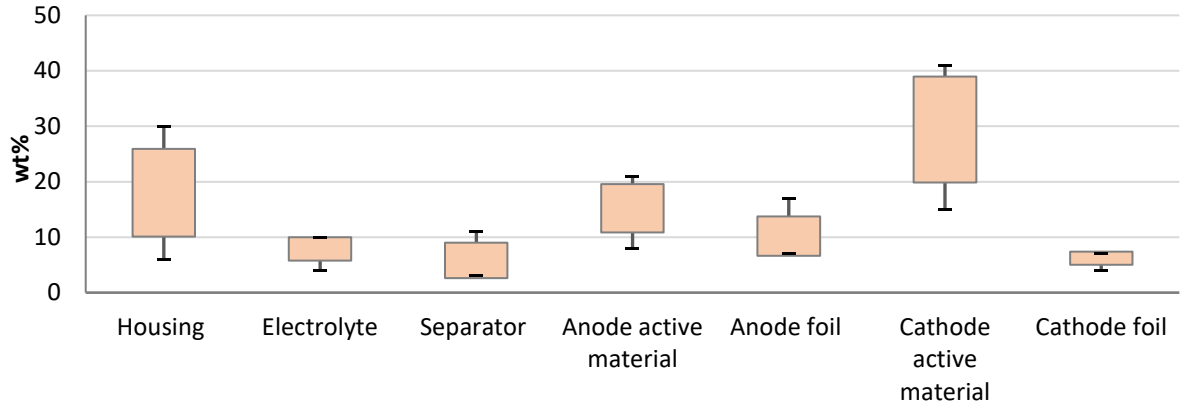

Figure 1: Generic composition of LiB cell in weight percentage (wt%) (mix LCO and NMC) [20–22]

2.2 Current recycling processes

The recycling of LiBs is still limited, and current processes focus more on the recovery of cobalt, nickel, or other metals, disregarding lithium. For instance, Global Electric Vehicle Outlook 2022 reports that the recycling rate for lithium is lower than 1% [3,12] and its official end-of-life recycling input in the EU is 0% [12]. However, it is very hard to obtain updated data and official statistics on the recycling LiBs and an even more precise recovery rate of the element. For instance, some Chinese media report that 30 to 40% of battery materials are recycled [23]. In 2019, in pv magazine, Hans Eric Melin, Director of Circular Energy Storage said, "We know from our data that about 100,000 tons of waste batteries were recycled last year, that's about 50% of what reached end-of-life" [24]. This section will explain briefly the existing recycling processes developed.

To create a sustainable and economically viable recycling process, the very first issue is the establishment of a good and robust collection and sorting system. The heterogeneity of the battery types available represents a major challenge to the setup of a performant collection infrastructure. Indeed, a very large variety of sizes, shapes, capacities, and battery chemical compositions can be found on the market [18]. The diversity of battery chemistry is the most challenging aspect, as not all recycling processes can handle every type of battery. Some decentralized collection and sorting points are emerging in Europe. This would be beneficial for the overall recycling framework. Implementation of rules such as the battery passport would also improve traceability, and thereby the collection of EV batteries.

2.2.1 Pre-treatment

Once the batteries are collected, they undergo different types of treatments. They are first, discharged for safety reasons, i.e., to avoid fire or electric shock. There are three predominant methods on the market: the use of salt-water baths (such as sodium chloride or sulphate), a controlled discharge by external circuits, and thermal treatment. The lithium ions move towards the cathode, making the spent cathode active material enriched in lithium [22].

Thermal treatment

Thermal treatment consists of applying relatively high temperatures (between 300°C and 700°C) under a controlled atmosphere. In the presence of airflow, it is called incineration, while pyrolysis is performed under an inert gas flow (argon or nitrogen). Such thermal treatment can also be performed under vacuum. The main advantages of applying a thermal treatment are the following:

1) The batteries can be inserted without preliminary discharge.
2) The decrease in waste volumes can help the transport, handling, and recycling of LiBs [25].
3) The binder decomposition allows easy separation of the active material from the current foils [18]. This also benefits the hydrometallurgical processes, as it concentrates the black mass and increases the contact surface between the valuable elements and the leaching agent.
4) The reduction of the complex metal oxides by carbon or carbon monoxide along with the formation of lithium carbonate. The latter is water-soluble and can allow selective lithium recovery before transition metals [11]. Moreover, the reduced oxides are more easily leached, which decreases the consumption of expensive reductants [26].

Mechanical treatment

The discharged batteries (with or without thermal treatment) undergo mechanical processing. The different components are separated based on the different physical properties, such as particle size, density, or conductive and magnetic properties. The main objective is to separate the metallic particles (casing, copper, and aluminium foils) from the cathode and anode active materials, a mixture called black mass [18]. Currently, the separators are removed from the battery waste, but they are disposed of instead of recycled. The price of the black mass then varies depending on the specific content of lithium, cobalt, nickel, manganese, and other materials [27]. Thus, the higher the concentration of valuable metals in the black mass, the more valuable it is.

2.2.2 Pyrometallurgical route

Current pyrometallurgical processes produce an alloy containing cobalt, nickel, copper, and iron, since those elements have a low oxygen affinity. This alloy must be further treated using hydrometallurgical techniques to separate the metals. Lithium, aluminium, and manganese have a high oxygen affinity and are transferred to slag [6,28]. Besides, there may be some lithium present in the flue dust stream due to the low vapour pressure of lithium compounds, such as lithium metal, lithium fluoride, and lithium carbonate, along with some volatile elements and fluorinated compounds. All carbon and organic compounds are burnt and leave the furnace as off-gases (CO and CO_2) [29].

One of the major advantages of pyrometallurgical processes is that they can handle a large volume of battery waste. They also provide high flexibility in term of the input material, since there is no need to sort collected batteries based on their chemistry (different LiBs or NiMH). Moreover, the spent batteries can be put in the furnaces without any prior discharging step or mechanical treatment. As an example, Umicore (Belgium) is currently recycling batteries using a

pyrometallurgical treatment called ultra-high temperature (UHT), and recovering nickel, cobalt, and manganese salt using a hydrometallurgical process after smelting [30].

However, the need for energy in such a process is concerning, and various gases are emitted. Furthermore, depending on the operating parameter, lithium is distributed among the flue dust and slag. Currently, it is not industrially recovered and is thus considered to be “lost”. Research for lithium recovery from those phases using hydrometallurgy is ongoing. Nevertheless, a feasible process is not expected in the coming years, as it will require high energy and chemical consumption due to the complexity of the slag [29].

2.2.3 Hydrometallurgical route

Compared to the pyrometallurgy route, hydrometallurgy methods make it possible to achieve higher recovery rates and require lower energy consumption. But it is a more complex and chemically intensive process. In traditional hydrometallurgical processes, the black mass from spent LiBs (obtained after discharging, dismantling, crushing, and sorting) is dissolved in inorganic acids. The metals present in the black mass are then dissolved in the leaching media. Usually, the addition of a reducing agent is needed to reduce the element into a more leachable oxidation state, i.e., from cobalt (III) to cobalt (II). The most common acid and reducing agents used are sulfuric acid and hydrogen peroxide, respectively [22]. The leaching conditions vary depending on the process chosen. The possible range parameters are as follows: acid concentration from 1 to 5 M, hydrogen peroxide addition from 3 to 10 vol%, temperature from 50 to 90°C, time from 1h to 6h, and a solid to liquid ratio (S/L) from 20 to 200 g/L [7]. The use of these inorganic acids is associated with various emissions (release of gas such as, SO_x, Cl_2, or NOx depending on the acid used) and the formation of waste streams and wastewater [20]. Some research is therefore ongoing in the replacement of the inorganic acid with an organic acid (citric, malic, or oxalic acid), avoiding gaseous emissions. They are usually considered more environmentally friendly than classic inorganic agents [20,31].

Leached metals are selectively recovered and purified using different techniques such as solvent extraction, ion exchange, precipitation, or crystallization. At first, impurities such as aluminium, copper, and iron are removed usually using sodium hydroxide, with the metals precipitated as hydroxide. However, other elements such as cobalt or lithium, can be co-precipitated during this operation. Hence, some research is being done in the use of techniques like ion exchange or solvent extraction to decrease the loss in that stage [22].

Next, nickel, cobalt, and manganese can be separated using solvent extraction or precipitation. Solvent extraction techniques separate the metal ions using organic extractants such as D2HPA, Cyanex 272, Acorga M5640, PC-88A, TODGA, or P66614-Cl [7]. One possible process is the use of D2EPHA to recover manganese from the leachate (common operation parameter: 0.5 M of the extractant at a pH of 2–2.5) [18]. Cyanex 272, an organophosphorus acid extractant, is then frequently used in the mineral industry for the separation of cobalt from nickel in sulphate solutions. Cobalt is extracted at a pH of about 5, while nickel is efficiently recovered at a pH of about 6.5 [18]. Their main disadvantage is the complexity of such a method, with multiple extraction stages, and the high cost of solvent, which in many cases is toxic [22]. Another method is the precipitation of the metals. The chemicals used can be lithium and sodium hydroxide, or

carbonate. The pH control required for an operation of this kind is often complicated, and co-precipitation of other elements can occur. For instance, lithium losses can be up to 25% in total, when using sodium hydroxide (pH = 11) [22].

Finally, lithium is recovered using sodium carbonate as precipitating agent (about 2 kg of sodium sulphate is generated for every 1 kg of lithium carbonate produced). A significant amount of sodium sulphate is generated as secondary waste, which currently has no utilization and is disposed of. Since lithium is obtained at the end of the recycling flowsheet, different extraction steps lead to lithium losses. This results in lower lithium recovery.

2.3 State-of-the-art in early recovery of lithium from LiBs

As seen in the previous section, current recycling systems do not have a high lithium recovery rate. Pyrometallurgy does not allow its recycling, while the current hydrometallurgy processes exhibit lithium losses. Usually disregarded, there has not been a major push to develop a recycling process centred around lithium. The existing recycling processes are more focused on expensive elements like cobalt or nickel. New recycling strategies are trying to lift the importance of lithium, which is gaining value on the market. This will be a good incentive for recyclers. One way to achieve this is to recover lithium in the first step in the hydrometallurgical flowchart. The main drivers in the use of this procedure are:

1) Improvement of overall lithium recovery.
2) Recovery of transition metals together without further separation.
3) Lower number of operation steps and thus lower cost of the recycling.

Two approaches can enable this early and selective recovery of lithium. The research outcome in this field will be described further. The improvement and better understanding of selected methods is the main focus of the present research project.

2.3.1 Combination of pyro and hydrometallurgy

In this approach, the black mass is thermally treated, followed by a water leaching. Lithium carbonate, produced during the metal oxide reduction, is dissolved selectively in the water while nickel, cobalt, and manganese remain in the solid phase. Lithium carbonate crystals are then obtained after evaporative crystallization at 95°C. Some authors have investigated this technique, and the parameters corresponding to the optimal leaching yield of lithium are summarized in Table 1. It can be observed that a high recovery rate is expected using this technique (between 60 to 95%), which makes it a very promising technique. Xiao et al. [32] investigated the variation in the leaching yield based on different cathode materials. It was shown that lower recovery was obtained for pure NMC material. All the optimal operating temperatures remained below 700°C, and the decomposition of lithium carbonate occurred over that limit. In fact, Maroufi et al. showed that at 800°C, all the lithium was liberated from the sample in the form of the gas [33]. However, the use of cold water did not have a positive influence on the dissolution.

Table 1: Summary of conditions for lithium dissolution after thermal treatment and water leaching reported in the literature (commercial cathode material *)

Material		**Initial composition (wt%)**	**Thermal treatment**				**Leaching**		**Li Yield (%)**	**Ref.**
Active material	Reducing agent		Type	Temp. (°C)	Time (min)	S/L (g/L)	Temp. (°C)	Time (min)		
$LiMnO_2$	Anode material	4.8 % Li, 0.1 % Ni, 51 % Mn	INC	650	60	40	Amb.	20	83	[34]
$LiMn_2O_4$ $LiCoO_2$ NMC	Anode material	-	Vacuum PYRO	700	45	40	Amb.	30	82 83 66	[32]
*NMC 111	10% Coke	7.2 % Li, 20.0 % Ni, 20.5 % Co, 19.4 % Mn	PYRO	650	30	34	25	60	94	[35]
LCO	20% activated carbon	6.5 % Li, 1.6 % Ni, 40.6 % Co, 1.6 % Mn, 7.8% Al	PYRO	700	30	-	0	60	36	[33]
NMC	Anode + 10% of graphite	2.2 % Li, 6.2 % Al	PYRO	700	60	50	80	180	60	[36]

2.3.2 The use of oxalic acid

The black mass obtained after mechanical treatment is directly treated with the acidic leaching. The most common organic acid used for lithium recovery is oxalic acid. The oxalic acid represents a good candidate as a leaching agent and acts as reducing agent. Moreover, it forms strong chelate complex with the metals which makes the mechanism of dissolution acid/complex based. Lithium reacts with oxalate ion to form a simple oxalate, while copper, cobalt, manganese, and nickel are reported to form simple and complex oxalates. However, it is more predictable to find simple oxalates for these metals [37].

Some authors have investigated this technique, and the main parameters leading to the optimal leaching yield of lithium are summarized in Table 2. Chrul-Kyoung L. et al. reported that with 3 M oxalic acid, at 80°C for 90 min and a solid-to-liquid ratios (S/L) of 50 g/L, all the lithium was dissolved, and less than 1% of cobalt was found in the leachate as insoluble CoC_2O_4 without using any addition of reducing agent [38]. Renjie Chen et al. [39] showed that the leaching behaviour with NMC cathode material differed slightly from the behaviour with LCO material. The authors observed the presence of NMC in the leaching residue even after more than 2 hours of operation, and the leaching yield of lithium was limited to 81%. They indicated that a morphology change and size increase of the aggregate NMC oxalate formed during the process with the leaching time. It was concluded that products were covering some remaining NMC oxides, and they were preventing the reaction. Moreover, they identified a higher concentration of manganese oxalate in the leachate solution, as it has a higher solubility than cobalt and nickel oxalate. However, less than 1.5% of the NMC was found in the leachate [39]. Ka Ming et al. [40] also investigated NMC leaching with oxalic acid. They demonstrated the co-dissolution of manganese, at the optimum leaching parameters (Table 2). Approximately, 96% of lithium was dissolved along with 24% of manganese. Increasing acid concentration and temperature led to an increase in the manganese extraction. Unfortunately, the effect of time on the leaching behaviour was not studied and very long dissolution times were applied (12 h).

Table 2: Summary of conditions for lithium dissolution using oxalic acid (OA) as a leaching agent reported in the literature

	Preparation of the feed material	[OA] (M)	S/L (g/L)	Temp. (°C)	Time (min)	Stir (rpm)	Leaching yield (%)				Ref
							Li	Co	Ni	Mn	
LCO	LCO powder from cathode and anode after crushing and magnetic separation (18mesh)	3	50	80	90	300	99	0.4	-	-	[38]
LCO	Discharged, crushed by shear crusher, and sieved (size <1.43mm)	1	15	95	150	400	98	< 3	-	-	[41]
NMC	Dismantling and manual separation of the anode and cathode. Cathode foil treated with NMP to recover active material. Pyrolysis at 700°C.	0.6	20	70	120	-	81	< 1.5	< 1.5	< 1.5	[39]
NMC	Commercial NMC (111, 532, 811)	1	10	95	12h	-	96	< 0.5	< 0.5	22	[40]

2.3.3 Conclusion on the early recovery of lithium and reasoning for a research scope

The two approaches seem to be very promising and could lead to increased lithium recovery.

In approach 1, promising recovery rates, of up to 90%, can be expected. However, some specification is needed to improve the method and understand the process. Different thermal treatments (incineration and pyrolysis) are applied with different sources of carbon (from the anode, graphite, coke, or lignite) to achieve better transformation of lithium to carbonates. However, the suitability of the carbon additives needs to be clarified. Incineration and pyrolysis will be investigated to define which is the more suitable for the operation. One important source of carbon in the battery cell is the separator, which is usually removed in the recycling process. Its effect in the carbothermic reduction has not been studied, but will be investigated in this work. Moreover, synthetic cathode materials are mainly used in all studies. Hence, there is a lack of information about the effects of the impurities present in real spent LiBs over the process. Impurities such as fluoride can change the outcome of the operation by reacting with lithium. Furthermore, the behaviour of other elements, such as copper or aluminium, is not reported. Finally, the purity of lithium carbonate recovered after evaporative crystallization is not investigated nor reported.

In approach 2, the different studies conducted previously identified the parameters influencing the leaching operation, such as reaction time, temperature, acid concentration, and solid-to-liquid (S/L) ratio. Very high lithium recovery is expected, up to 98%, without the use of thermal treatment or a reducing agent. This constitutes a big advantage for the recycling process. The co-extraction of manganese is reported at different levels. However, research with the industrial black mass would allow a better estimation of the co-dissolution. Finally, the behaviour of other elements, such as copper or aluminium, is not reported.

This research will focus on achieving maximum recovery of lithium, with a deeper understanding of the processes since both approaches will be investigated.

3 Theory

3.1 Carbothermic reduction during the thermal treatment

3.1.1 Principle

The carbothermic reduction is described as the reduction of oxide metals (written MO in the equation) to a lower oxidation stage using carbon as a reductant. The main reaction products are reduced metals, CO, and CO_2. This phenomenon occurs above 500°C and below 700°C [42], following the subsequent Equation 1 and 2. Over 700°C, CO becomes pre-dominant.

$$3\,MO_s + 2\,C_s \rightarrow\ 3\,M_s +\ CO_g +\ CO_{2,g} \quad (1)$$

$$MO_s +\ CO_g \rightarrow\ \ M_s +\ CO_{2,g} \quad (2)$$

The black mass can contain from 10 to 45 wt% of graphite and carbon [22]. This is a good source of carbon for the carbothermic reduction. Another additional source of carbon can come from the organic solvent present in the electrolyte and the separator, which is made mainly of PP and PE. The black mass can contain from 3 to 10 wt% of separator [22]. Beyond a temperature of 500°C, the PP and PE undergo a complete decomposition forming, CO, CO_2, and H_2O. Hence, no additional contaminants are expected when the separator is processed with the rest of the cell.

3.1.2 Incineration

Incineration involves mostly exothermic reactions [25]. During the incineration, the presence of oxygen causes the combustion of graphite and organic components to form CO and CO_2 (Equations 3–5) [47]. The formation of the latter is favoured at a temperature below 700°C. The metal oxides are reduced under the reducing atmosphere. $LiCoO_2$ is reduced by C and CO and formed Co_3O_4, Li_2CO_3, CoO, and CO_2. $LiMn_2O_4$ is reduced to Mn_3O_4, MnO_2, MnO, and Li_2CO_3. $LiNiO_2$ had the same behaviour as $LiCoO_2$ and is reduced to Ni_3O_4, Ni, and NiO. The formation of lithium carbonate comes from the reaction between the Li_2O, product of the carbothermic reduction, and the CO_2 [25].

$$C_s +\ O_{2,g} \rightarrow\ \ CO_{2,g} \quad (3)$$

$$C_s +\ {}^1\!/_2\ O_{2,g} \rightarrow\ \ CO_{\,g} \quad (4)$$

$$2\,CO_g +\ O_{2,g} \rightarrow\ 2\,CO_{2,g} \quad (5)$$

$$Li_2O_s +\ CO_{2,g} \rightarrow\ Li_2CO_{3,s} \quad (6)$$

3.1.3 Pyrolysis

Pyrolysis is reported to involve mostly endothermic reactions [25,43]. During pyrolysis, the carbon present in the samples triggers the carbothermic reduction of the metal oxides [49]. $LiCoO_2$ is reduced by C and CO and formed Co, CoO, and Li_2O which reacted with the CO_2 produced to form Li_2CO_3 (Equations 7–10). $LiMn_2O_4$ is reduced to Mn_3O_4, MnO, Li_2O, and Li_2CO_3 (Equations 14–18). $LiNiO_2$ has the same behaviour as $LiCoO_2$ and is reduced to Ni and NiO (Equations 11–13). Less CO_2 is emitted during the operation, which is therefore considered a more sustainable process than incineration.

$$16\,LiCoO_{2,s} + 10\,C_s \rightarrow\ Co_3O_{4,s} + CoO_s + 12\,Co_s +\ 8\,Li_2CO_{3,s} + CO_{2,g}\ + CO_g \quad (7)$$

$$LiCoO_{2,s} + CO_g\ + 3/10\,C_s\ \rightarrow\ 3/10Co_3O_{4,s} + 3/10CoO_s + 9/10\,Co_s +\ Li_2CO_{3,s} + 3/10\,CO_{2,g} \quad (8)$$

$$9/10Co_3O_{4,s} + 34/25C_s + CO_g\ \rightarrow\ 14/5\,Co_s +\ 12/5CO_{2,g} \quad (9)$$

$$3CoO_s + C_s + CO_g\ \rightarrow\ 3\,Co_s +\ 2CO_{2,g} \quad (10)$$

$$8\,LiNiO_{2,s} + 6\,C_s \rightarrow\ NiO_s + 7\,Ni_s +\ 4\,Li_2CO_{3,s} + CO_{2,g}\ + CO_g \quad (11)$$

$$LiNiO_{2,s} + CO_g\ + 2/3C_s\ \rightarrow 2/3NiO_s + 4/3Ni_s +\ Li_2CO_{3,s} + 2/3CO_{2,g} \quad (12)$$

$$3NiO_s + C_s + CO_g\ \rightarrow\ 3\,Ni_s +\ 2CO_{2,g} \quad (13)$$

$$10\,LiMn_2O_{4,s} + 7C_s \rightarrow\ Mn_3O_{4,s} + 16\,MnO_s\ +\ MnO_{2,s}\ +\ 5Li_2CO_{3,s} + CO_{2,g}\ + CO_g \quad (14)$$

$$2LiMn_2O_{4,s} + 0.5C_s + CO_g\ \rightarrow\ 0.5Mn_3O_{4,s} + 2MnO_s\ +\ 0.5MnO_{2,s}\ +\ Li_2CO_{3,s} + 0.5CO_{2,g} \quad (15)$$

$$2Mn_3O_{4,s} + C_s \rightarrow\ 6MnO_s\ +\ CO_{2,g} \quad (16)$$

$$Mn_3O_{4,s} + CO_g\ \rightarrow\ 3MnO_s\ +\ CO_{2,g} \quad (17)$$

$$3MnO_{2,s}\ + C_s +\ CO_g\ \rightarrow\ 3MnO_s\ +\ 2CO_{2,g} \quad (18)$$

The thermal decomposition of PVDF is influenced by the oxygen content. An increase in the proportion of oxygen in the atmosphere decreases the maximum rate of decomposition slightly but has a larger effect on the temperature at which initial decomposition occurs. Decomposition under oxygen occurs at 320°C, while it starts at 450°C under nitrogen [44]. The main product of decomposition is hydrofluoric acid (HF) in the gas phase. The generation of hazardous gaseous substances such as HF requires that the off-gas is cleaned, hence HF is trapped and neutralized with water.

During the thermal treatment, the lithium salts in the electrolyte, such as $LiPF_6$, can decompose into lithium fluoride and HF at a temperature higher than 200°C in the presence of water [6].

$$LiPF_6 +\ H_2O \rightarrow LiF(s) + POF_3(g) + 2HF(g) \quad (19)$$

Moreover, the gaseous HF formed can react with Li_2O or Li_2CO_3 to form lithium fluoride (Equations 20–21). At 600°C, those reactions are spontaneous with a Gibbs Free Energy (ΔG) of -224.2 kJ and -135.0 kJ, respectively [1].

$$Li_2O\ +\ 2\,HF\ (g) \rightarrow\ 2\,LiF\ +\ H_2O\ (g) \quad (20)$$

$$Li_2CO_3 +\ 2\,HF\ (g) \rightarrow\ 2\,LiF\ +\ H_2O\ (g)\ +\ CO_2\ (g) \quad (21)$$

[1] HSC Chemistry 9 developed by Outotec was used to calculate the thermodynamic data.

3.2 Leaching

3.2.1 General principle

The goal of the leaching operation is the dissolution of a desired element, contained in a solid phase, into a liquid media. The leaching agent is selected for its ability to dissolve the metals contained in the black mass; the metals are leached into the solution which is then called "leachate". The probability of an element leaching can be evaluated by considering the leaching mechanism; it can be oxidative or reductive leaching as well as simple chemical dissolution. The choice of leaching agent is also important for the rest of the process. For instance, if solvent extraction is applied to further separate the element in the solution, the nature of the solution is very important. The main driving parameters of such an operation are the temperature, S/L ratios, concentration of the leaching agent, rotation speed, and time. The kinetics of the dissolution can be investigated by measuring the leached amount of the element of interest at various points in time. The industrialized process generally appreciates low reaction time, as it is usually more profitable for their activity.

The leaching yield (%Y) can be calculated by comparing the concentration of each element in the leachate to the elemental content of the solid samples determined by the total dissolution in aqua regia. The leaching efficiency can be calculated according to Equation 22:

$$\%Y_i = \frac{C_i \times V}{m_0 \times w_i} \times 100 \quad (22)$$

where C_i is the concentration of the element *i* in the leachate (mg/L), V is the volume of solution (L), m_0 is the weight of the sample (mg) and w_i is the weight percentage of the element *i* in the sample (%).

The purity of the leachate (%P) can be calculated using Equation 23:

$$\%P_i = \frac{C_i \times V}{C_i \times V + \sum_j C_j \times V} \times 100 \quad (23)$$

where C_i is the concentration of the element *i* in the leachate (mg/L), C_j is the concentration of any other elements, *j*, found in the leachate (mg/L) and V is the volume of solution (L).

3.2.2 Water leaching of thermally treated solid

This operation relies on the dissolution of lithium compounds in water. The solubilities of certain lithium compounds are given in Table 3. Lithium carbonate is the main lithium compound formed in the thermal treatment. Another compound formed during the thermal treatment is Li_2O, which will spontaneously react with water to form lithium hydroxide (Equation 24 - ΔG° negative).

$$Li_2O + H_2O \rightarrow 2\,LiOH \quad (24)$$

Lithium fluoride is almost insoluble in water. The production of lithium fluoride may therefore limit lithium extraction with water.

Table 3: Solubility of lithium compounds [45]

	Li_2CO_3	LiOH	LiF
Solubility (g/L) at 20°C	13.3	110	1.2
Solubility (g/L) at 100°C	7.2	161	1.3

3.2.3 Oxalic acid leaching

Oxalic acid forms strong chelating agents which make the mechanism of dissolution acid/complex based. Lithium reacts with oxalate ion to form a simple oxalate, while copper, cobalt, manganese, and nickel are reported to form simple and complex oxalates. However, it is more predictable to find simple oxalates for these metals [37]. The main dissolution reactions, for the leaching of LCO cell, are identified as observed in Equations 25–26 [41,46]:

$$4\,H_2C_2O_4 + 2LiCoO_2 \rightarrow Li_2C_2O_4 + 2CoC_2O_{4\,solid} + 4H_2O + 2CO_{2\,gas} \quad (25)$$

$$7\,H_2C_2O_4 + 2LiCoO_2 \rightarrow 2LiHC_2O_4 + 2CoC_2O_{4\,solid} + 4H_2O + 2CO_{2\,gas} \quad (26)$$

Oxalic acid excess is also characterized as observed in equation (27–28–29) [41]. Aluminium extraction can occur in the case of oxalic acid excess, as seen in Equation 29.

$$H_2C_2O_4 + Li_2C_2O_4 \rightarrow 2\,LiHC_2O_4 \quad (27)$$

$$H_2C_2O_4 + CoC_2O_{4\,solid} \rightarrow 2Co(HC_2O_4)_{2\,liquid} \quad (28)$$

$$3\,H_2C_2O_4 + Al \rightarrow Al(HC_2O_4)_3 + {}^3/_2\,H_{2\,gas} \quad (29)$$

Hence, the selectivity of the operation lies in the precipitation capacity of certain oxalates. Manganese, nickel, and cobalt oxalate are expected to remain in the solid phase due to their low solubility, while lithium should be dissolved, as this can be anticipated from the solubilities data reported in Table 4. Aluminium, on the other hand, is reported to form only complex oxalate compounds which are soluble in aqueous media, thus, consequent dissolution is expected.

Table 4: Solubility and solubility product constant (K_{sp}) of oxalate compounds [47]

	$Li_2C_2O_4$	CuC_2O_4	MnC_2O_4	CoC_2O_4	NiC_2O_4
Solubility (g/L) at 18°C	6.6	-	-	0.035	0.003
K_{sp}	-	$4.4.10^{-10}$	$1.70.10^{-7}$	$5.7.10^{-8}$	$4.2.10^{-10}$

4 Materials and methods

4.1 Black mass

Material 1 (used in Approach 1)

Pouch NMC batteries, provided by Volvo Cars, were manually dismantled, and both the electrodes and the separator were cut into 2 mm pieces before being thermally treated. This process is illustrated in Figure 2.

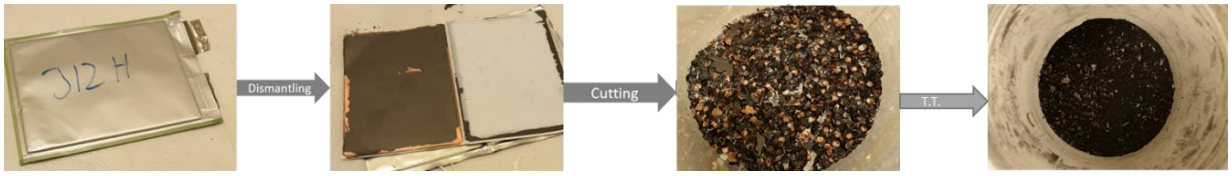

Figure 2: Sample preparation, from discharged battery to thermally treated sample.

Material 2 (used in Approach 1 and 2)

The black mass used for this study was obtained from the dismantling of 150 kg EV spent lithium-ion batteries provided by Volvo Cars AB (Sweden). The battery packs were discharged by Volvo Cars AB and then dismantled down to the cell level by Stena Recycling AB in Sweden. The chemistry of the battery cells was NMC 111. The cells (120 kg) were then processed through three steps: crushing, mechanical sieving, and magnetic separation by Akkuser Oy (Finland). The processing temperature stayed below 50°C. The fine fraction obtained represents 58.5% of the initial weight and is composed of the active materials from the cathode and anode along with the current foils and separator.

The fine fraction was further sieved under 500 µm in the Industrial Materials Recycling group at Chalmers University of Technology (Sweden) to obtain a very homogeneous powder. The main scope was to concentrate the active material and further remove the current collector foils. The sieving of the black mass was performed with a sieve shaker (Retsch) for 5 minutes at an amplitude of 1.2 mm in interval mode and a sieve aperture of 500 µm.

4.2 Chemicals

The chemicals used in this work are listed below:

- HCl Merk Millipore Chloric acid 37% w/w used for solid digestion.
- HNO_3, Merk Millipore Nitric acid 65% w/w used for solid digestion.
- HNO_3 (Merk Suprapure Nitric acid 69% w/w) for ICP dilution.
- Oxalic acid was prepared by dissolving solid oxalic acid dihydrate (Sigma Aldrich, ≥99%) in Milli-Q water.
- Milli-Q water (18.2 MΩ•cm) was used for all aqueous dilutions.
- Buffer solution pH 2.00, 4.00, 7.00 (20°C) (Sigma Aldrich – Certipur)
- TISAB IV solution for fluoride determination (Sigma Aldrich)
- Fluoride ion solution for ISE 0.1 M in fluoride, analytical standard (Sigma Aldrich)

4.3 Equipment

4.3.1 Thermal treatment setup

Thermal treatments were performed in a horizontal tube (high purity alumina tube 65 cm alumina tube Degussit AL23 Aliaxis) furnace (Nabertherm GmbH Tube furnace RT 50-250/13), as shown in Figure 3. The samples were held in an alumina crucible. Two different types of thermal treatment were performed: active pyrolysis under constant pure nitrogen flow of 340 mL/min and incineration under 340 mL/min of air. The exhaust gases were washed through the washing system based on the plastic-sealed bottles containing Milli-Q water. The main scope was to neutralize the HF formed during the processing.

Figure 3: Furnace setup [21]

4.3.2 Leaching setup

Two types of leaching reactors were used for this work. Small glass vials with caps and magnetic stirrers (300 rpm) 20 mL in size were used for the preliminary experiments. The temperature was sustained via a heated aluminium block in which glass vials were inserted and control of the temperature was monitored via a thermocouple (Figure 4a). The other option was a 100 mL double-enveloped reactor with electric agitation for upscaled experiments (Figure 4b). In both cases, solid samples were introduced in the reactors when the leaching media had reached the defined temperature. In addition, the obtained slurry was filtered using filter VWR 516-0811 – 11 µm particle size retention. All experiments were carried out in triplicate.

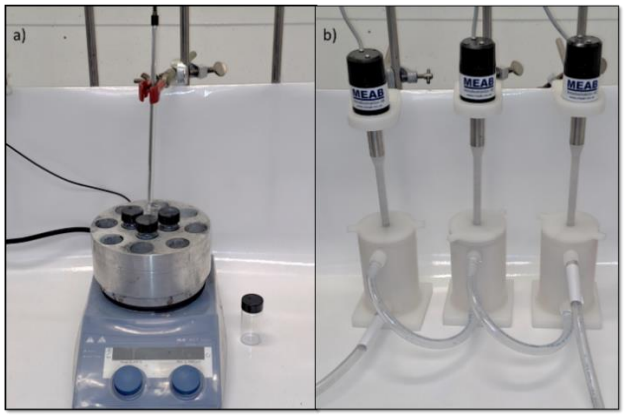

Figure 4: Leaching reactor set up for small volume (20 mL - a) and large volume (100 mL - b).

4.3.3 Analytical tool for liquid phase characterization

Inductively coupled plasma-mass spectrometry

The concentration of lithium, aluminium, copper, nickel, cobalt, and manganese was measured using an inductively coupled plasma-mass spectrometer (ICP-OES, Thermo Fisher Scientific, Model iCAP™ 6000 Series). The samples were diluted with 0.5M HNO_3 in the linear range of calibration from 0.625 to 20 ppm. An approximate 0.1 ppm limit of detection was estimated for the method used.

Fluoride analysis

The concentration of fluoride was measured with a fluoride-selective electrode (Ion-selective electrode, F, Metrohm) along with a reference silver/silver chloride electrode with a double junction system. The liquid sample was mixed with TISAB IV solution (volume ratio 1:1) before measurement to keep the pH and ionic strength constant. The TISAB also bound with interfering cations and thereby releasing any complexed fluoride. Calibration was performed before each measurement.

pH electrode

The pH of the solution was monitored during the operation using a pH electrode (Metrohm 6.0258.600) connected to the Tiamo software to record the data. The electrode was calibrated with buffer solutions at pH 2, 4, and 7 before each experiment at 20°C.

4.3.4 Analytical techniques for solid phase characterization

Digestion of solid sample for elemental composition

The sampling was performed using the coning and quartering technique to divide an initial sample into halves until the desired sample weight was achieved. This procedure helps to reduce the uncertainty associated with grab sampling from a container [48]. To determine the metal composition of the material, aqua regia (HCl/HNO_3: 3/1 volume ratios) was used to digest the solid samples at 80 $^{\circ}$C for 4 h. The slurry was then left to cool down overnight. After filtration (filter VWR 516-0811 – 11 µm particle retention) and dilution in HNO_3 0.5 M, the metal content was analysed using ICP-OES with the same method as presented above.

X-ray diffraction

X-ray powder diffraction (XRPD, Siemens D5000 diffractometer) was used to characterize the solid samples using a Cu (λ = 1.54184 Å) radiation source, in a 2θ range of 10°–80° with a rotational speed of 15 rpm. The operating current and voltage used were 40 mA and 40 kV respectively. EVA software and the JCPDS database were used for analytical interpretation.

Carbon analysis

A LECO CS744 instrument was used to determine the carbon content in the samples before thermal treatment. Approximately 20 mg of sample was weighed out in an alumina vial and introduced in the machine to be oxidized to CO_2, which was then measured by an infrared detector. Oxygen was measured in a LECO TC-436DR analyser. Oxygen reacts with the crucible to form CO_2 which was measured with non-dispersive infrared cells. Measurements were done in triplicate to estimate the measurement uncertainties in the instruments.

Fourier-transformed infrared spectroscopy (FT-IR)

FT-IR (Perkin Elmer Spectrum Two UATR) was used to analyse the powder over the range of 450 to 4000cm^{-1} with a resolution of 2cm^{-1} and 16 scans.

4.4 Design of experiments

A factorial design of experiments can be used to optimize a chemical operation. The use of this methodology allowed the optimization of the experimental efforts. It is based on the assessment of the main parameters influencing the operation and modelling the process using a reduced number of tests. In addition, the response surface methodology, and contour plots can aid in the visual interpretation of the modelled responses.

The effect of each factor is defined to be the change in response produced by a change in the level factor [49]. Each factor (X) comprised two levels (2^3 factorial design), and the process response (Y) was defined as the leaching yield of each metal (%). To apply this method, the factors need to be fixed beforehand, and the test order is randomized.

The design matrix is presented in Table 5 following a cubic face-centred design, with axial points performed (2*k* axial points) at a distance of $\alpha = 1$ from the central point to enable estimation of second terms and curvature, highlighted in green in the table. At the central level, the design was replicated four times to estimate the experimental error, highlighted in red.

The coefficients of a linear second-order regression model representing the process response were fitted using the linear least squares method (second-order regression models with two- and three-way interactions), which was solved using Excel´s regression analysis tool. Only statistically significant variables were included in the models (*p*-value < 0.05) and the significance of the models was assessed using Analysis of Variance (ANOVA). The existence of pure curvature was evaluated by hypothesis testing, and the variance of the response accounted by the models was assessed by the coefficient of determination (R^2).

Table 5: Design matrix

Test Order		Coded variables		
Standard Sequence of tests	Random test sequence	x1	x2	x3
1	12	-1	-1	-1
2	11	1	-1	-1
3	3	-1	1	-1
4	6	1	1	-1
5	8	-1	-1	1
6	14	1	-1	1
7	4	-1	1	1
8	13	1	1	1
9	17	0	0	0
10	10	0	0	0
11	1	0	0	0
12	2	0	0	0
13	5	-1	0	0
14	18	1	0	0
15	15	0	-1	0
16	7	0	1	0
17	9	0	0	-1
18	16	0	0	1

5 Experimental procedure

The two different processes studied in this work are presented in Figure 5. Only the part frame in red is discussed in this thesis. The following section will detail the different operations and analyses performed.

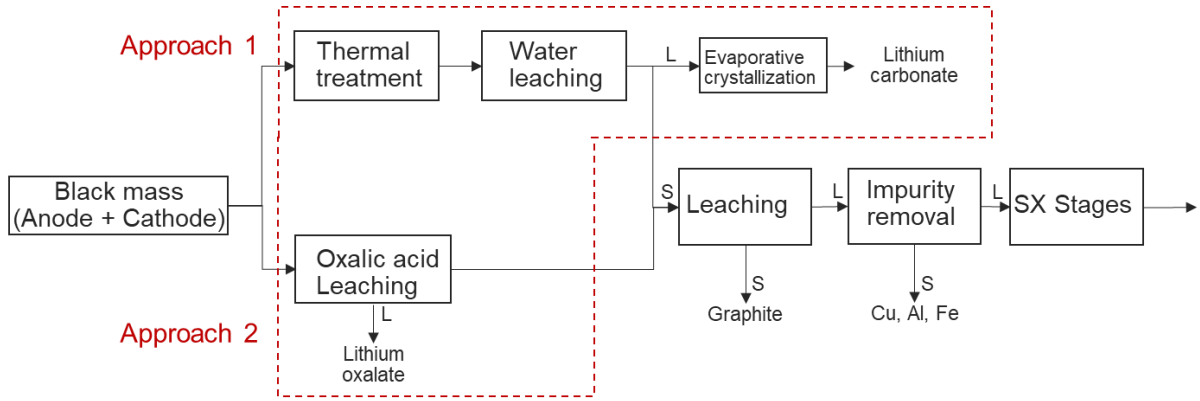

Figure 5. Workflow scheme for the proposed work.

5.1 Approach 1 (Paper I)

The solid samples were thermally treated in a horizontal tube furnace. Five grams of material were individually inserted into the furnace in an alumina crucible when the furnace was at the target temperature. Two different types of thermal treatment were performed: active pyrolysis (340 mL/min of N_2) and incineration (340 mL/min of air). Two input materials were studied, the cathode and anode with and without the separator foil. For each thermal treatment type, a range of temperatures between 400 °C and 700 °C were tested for 30, 60, and 90 minutes. Once the experiment was finished, the samples were cooled down in the furnace under the same atmosphere. After grinding with an IKA M20 universal mill for 5 minutes, the metal content and composition of the homogeneous solid residue were determined after digestion.

Water leaching was performed using Milli-Q water for each pre-treated sample with a S/L ratio of 20 g/L. This large excess of leaching agent was chosen to achieve the maximum lithium recovery after thermal treatment and to minimize the effect of the sampling. The experiments were performed in 20 mL glass vials with a cap. The sampling was performed using the coning and quartering technique to divide an initial sample into halves until the desired sample weight was achieved. The leaching temperature varied, and specific conditions are presented in the results section. After leaching, the samples were immediately filtered (Syringe filter PTFE – Restek – 0.45 µm) to separate the solid residue from the liquid phase containing the lithium salts. The metal content of each leachate was analysed using ICP-OES.

Once the leachate was separated from the solid residue, it was heated to 95°C to evaporate the water and collect the lithium salts. An elemental composition analysis of the obtained salt was performed using ICP-OES measurement after its dissolution in nitric acid. This powder was then analysed using XRD to identify the different components.

5.2 Approach 2 (Paper II)

Oxalic acid leaching experiments were performed in 20 mL glass vials with caps. After the leaching, the samples were immediately filtered to separate the solid residue from the liquid phase containing the dissolved metals, to avoid any precipitation that could occur. The metal content of each sample was analysed using ICP-OES.

The leaching optimization was achieved through a factorial design of experiments, response surface methodology, and contour plots that assisted in the visual interpretation of the modelled responses. The factors and respective levels used in this study can be observed in Table 6. The design factors are oxalic acid concentration, leaching time, and temperature. They were chosen based on the range of conditions from the literature review previously presented at the end of section 2.3.2. When using such an approach, setting a representative working range of conditions was prioritized, as the model obtained is only valid within the experimental limits. The S/L ratio was fixed at 50 g/L to have sufficient dispersion of the slurry and efficient mixing. Black mass samples were obtained through the quartering method.

Table 6: Factors and respective levels considered in the factorial design of experiments.

Factors	**Levels**		
	Low (-1)	Center (0)	High (+1)
Oxalic acid concentration (M) (x_1)	0.3	0.6	0.9
Leaching time (min) (x_2)	15	60	105
Leaching temperature (°C) (x_3)	35	50	65

A scale-up of the experiments was realized with a double-enveloped PVDF reactor of 100 mL, on the optimal parameter obtained in the design. Samples (0.25 mL) were taken after 1, 3, 5, 10, 30, 60, 90, and 105 minutes and immediately filtered and diluted for ICP–OES analysis. The pH of the solution was monitored during the operation. When the test was completed, the solid residue was collected after filtration and dried for 24 h in an oven (50°C) for further material characterization. XRD and FT-IR were used to characterize the solid samples and ICP-OES was used on the dissolved residue.

6 Results and discussions

6.1 Approach 1

6.1.1 Characterization of the solid samples

The metal composition and carbon content of the black mass, with and without the separator foil, before thermal treatment is presented in Table 7. The total carbon content without separator (Material 2) measured at 22.6%, and a clear increase of carbon content could be seen with the presence of separator (Material 1), measured at 40.8%. The carbon content of the separator alone was measured at 70% ± 3%.

Table 7: Metal and carbon composition (wt%) of the untreated black mass with (Material 1) and without (Material 2) the separator.

	***wt%* Li (%)**	***wt%* Al (%)**	***wt%* Cu (%)**	***wt%* Ni (%)**	***wt%* Co (%)**	***wt%* Mn (%)**	***wt%* C (%)**
Material 1	2.2 ± 0.2	6.2 ± 0.3	15.0 ± 0.4	4.3 ± 0.4	4.3 ± 0.4	9.5 ± 0.8	40.8 ± 2.8
Material 2	3.1 ± 0.1	9.5 ± 0.9	12.7 ± 3.8	6.3 ± 0.3	6.1 ± 0.3	13.8 ± 0.6	22.6 ± 0.8

6.1.2 Pre-investigation of water leaching conditions for untreated samples

To define the effect of thermal treatment, the water leaching of untreated Material 1 was performed at 3 different temperatures (25, 40, and 60°C).

Figure 6 The equilibrium was reached after 30 minutes, with maximum lithium recovery after water leaching at around 7.5%, as observed in Figure 6. In this case, the lithium found in the solution could only come from the $LiPF_6$ used in the electrolyte or from the reaction between water and the remaining Li_2O from the manufacturing process. No significant increase in lithium dissolution could be observed when applying the different leaching temperatures. Based on this observation, the following leaching experiments were performed at 25°C with a leaching time of 1 h. This choice of parameter is part of an approach to reduce the energy costs of the process, also considering that lithium carbonate is more soluble at a lower temperature. Kinetics studies will be performed on the optimal treatment to identify when the equilibrium is reached in the case of a treated sample.

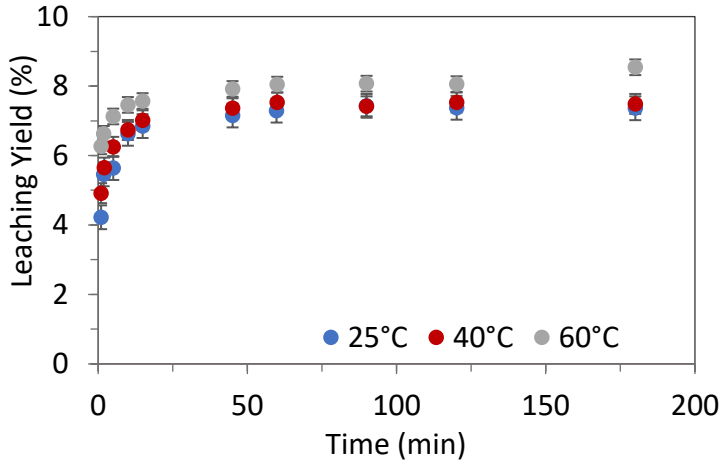

Figure 6: Lithium leachability (leaching yield) in water for an untreated sample (Material 1) at 25°C, 40°C, and 60°C at S/L = 20 g/L and stirring speed of 300 rpm.

6.1.3 Effect of thermal treatment on lithium leachability

When leaching thermally treated Material 1 (with the separator), it was confirmed that the presence of the separator had a positive influence on the carbothermic reduction of the oxides. In the case of Material 2 (without the separator), lithium recovery from thermally treated samples did not exceed 35% (Paper I). Temperature and time did not show any significant effect. It was thus confirmed that the presence of separator enhances the formation of lithium carbonate due to the presence of a higher carbon content. For this reason, only the black mass processed with the separator (Material 1) will be described further.

A general weight loss of 5 to 20% was observed after the thermal treatment (incineration and pyrolysis) for Material 1 [42,50], without any significant influence on the running parameters. This is due to the conversion of carbon, from solid phase to gas, when reacting with oxygen. The metal content increases after the thermal treatment, as the total mass of the sample was lifted from the carbon and oxygen loss.

The speciation of the obtained treated residue (from Material 1) was done by XRD, as presented in Figure 7. This confirms that the Material 1 was a mixture of NMC 111 cathode material and anode active material with their current collector. The increase in temperature during the thermal treatment induces the carbothermic reduction of the metal oxides. The peaks of NMC material decrease with temperature of the treatment, while the peaks of reduced oxides increase. Over 700°C, the metal oxide peaks disappear, and the lithium carbonate was determined.

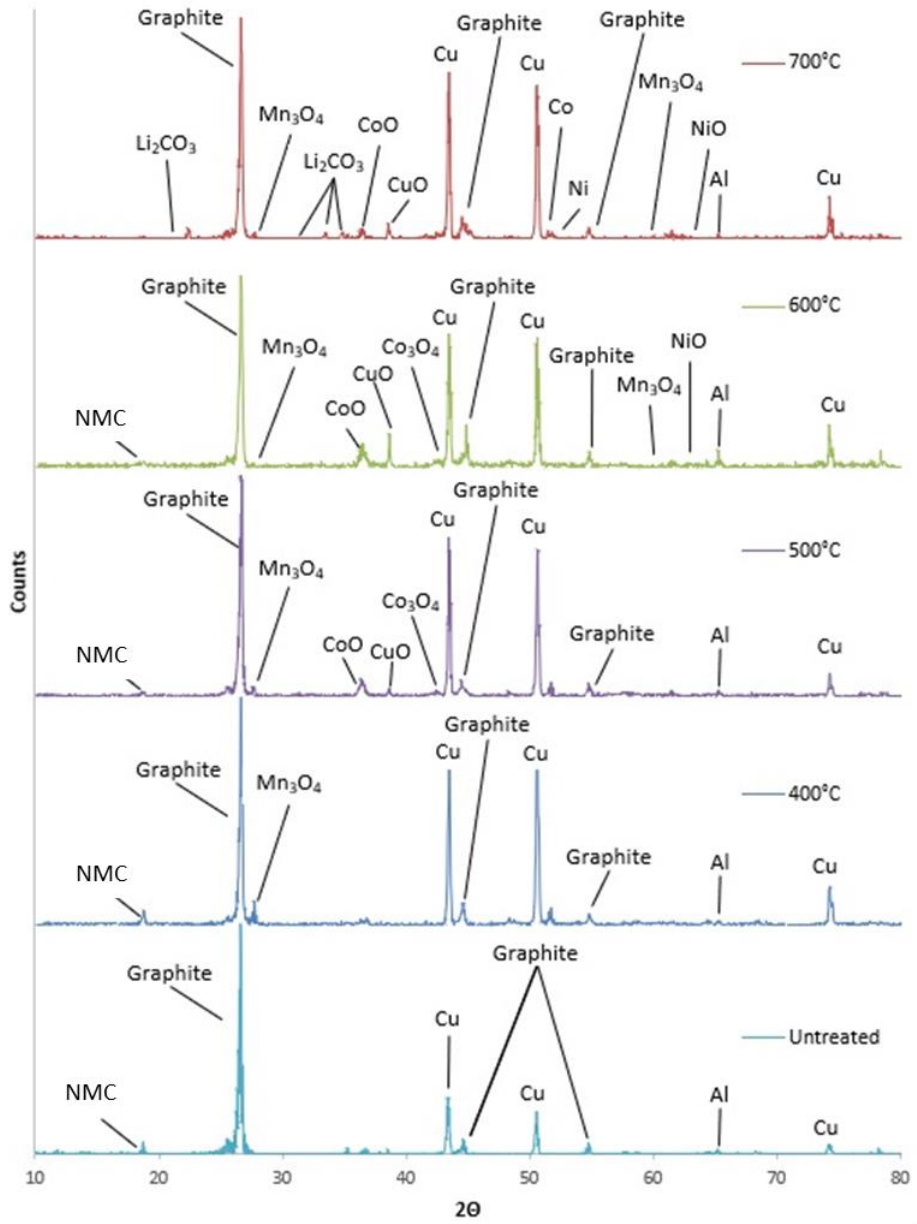

Figure 7: XRD pattern of the pyrolyzed sample at different temperatures [21]

Effect of incineration

At 400°C, the leaching yield is around 20%, which is only 10% higher than the untreated material as can be observed in Figure 8. The carbothermic reduction of the oxide occurs above 500°C, thus a more reductive atmosphere is provided beyond that temperature [25]. It was observed that the treatment time has no significant influence on the recovery of lithium. Shorter times will therefore be applied for further studies, thereby reducing the energy consumption. A significant decrease in efficiency is observed at 700˚C. Over 660˚C, aluminium melts and may coat the particles, making it even more difficult for the oxides to react with the gases and thus hindering their carbothermic reduction. This behaviour was also reported by others [25]. The results showed that water leaching is not completely selective to lithium and some aluminium is also leached. The

determined purity of the solution decreased when the treatment temperature increased regardless of the treatment time.

The optimal conditions observed using incineration are thermal treatment at 500˚C for 90 minutes, which leads to lithium recovery of 43% and solution purity of 90%. Under these conditions, the concentration of lithium and aluminium in the leachate was 215 mg/L and about 25 mg/L, respectively.

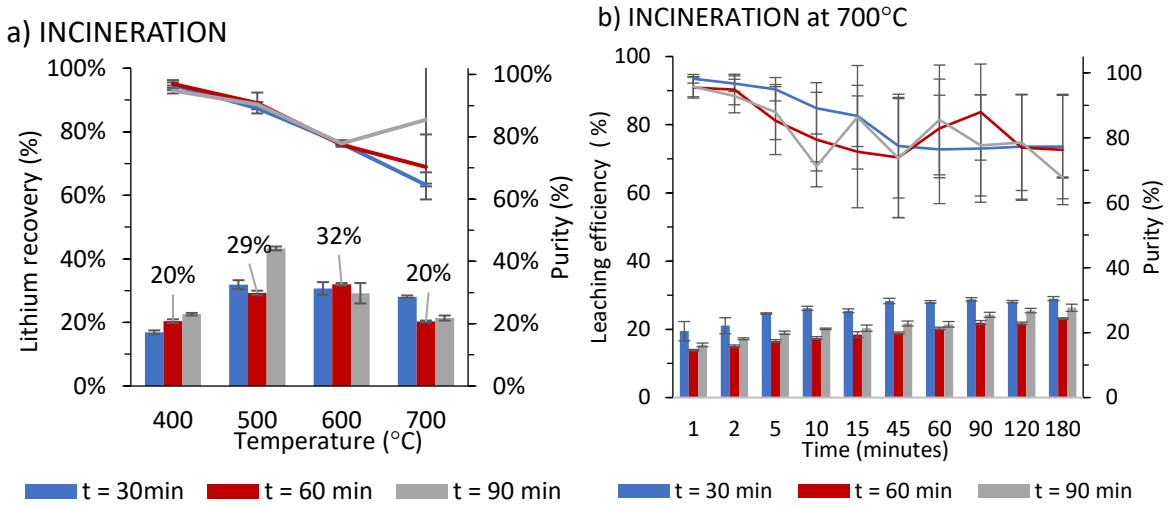

Figure 8: a) Lithium recovery (Left axis – histogram) and purity (Right axis – line) after incineration at different temperatures (400–700°C) and treatment time (30–90 min) followed by water leaching (S/L = 20 g/L, 25°C, 1 h, 300 rpm) and b) after incineration at 700°C for 3 different treatment times and water leaching at 25 °C, S/L = 20 g/L

Effect of pyrolysis

After pyrolysis at 400˚C, similar efficiencies were obtained for different treatment times with a recovery limitation of 20%, as can be seen in Figure 9. The same trend was obtained after incineration at low temperature, which supports the hypothesis concerning the absence of a reducing atmosphere under 500˚C. Moreover, the thermal decomposition of PVDF is known to occur at 450°C under a nitrogen atmosphere [44,48]. At 400°C, PVDF can still be partially present in the sample, which could prevent good contact between the particles and the leaching media (water). Finally, as seen in Figure 7, at 400°C and 500°C, the three lithium-metal oxides are still present in the black mass, thus the carbothermic reduction is not completed.

Unlike incineration, pyrolysis temperature seems to have a positive effect on recovery, with a gradual increase in the lithium leaching yield. There is no limiting factor, and the amount of lithium carbonate increases with treatment temperature. Prolonging the treatment time did not lead to an improvement in recovery. In this case, aluminium is also leached along with lithium. The purity decreases with an increase in treatment time and temperature. The dissolution of aluminium was not expected, nor it was reported previously. Identification of the aluminium water-soluble species formed in the thermal treatment could help to prevent its production. The hypothesis made so far is the reaction of the aluminium foils with HF, following the reaction

(Equation 30). This reaction is spontaneous at high temperatures, with a ΔG of -446.4 kJ at 600°C. Unfortunately, this could not be characterized by XRD, due to the detection limit of the method.

$$Al + 3\,HF_g \rightarrow AlF_3 + 1.5\,H_{2,g} \quad (30)$$

The final leachate purity is increasing for the samples processed at 700°C, which could indicate that aluminium is preferentially forming less water-soluble species over its melting point (at 660°C).

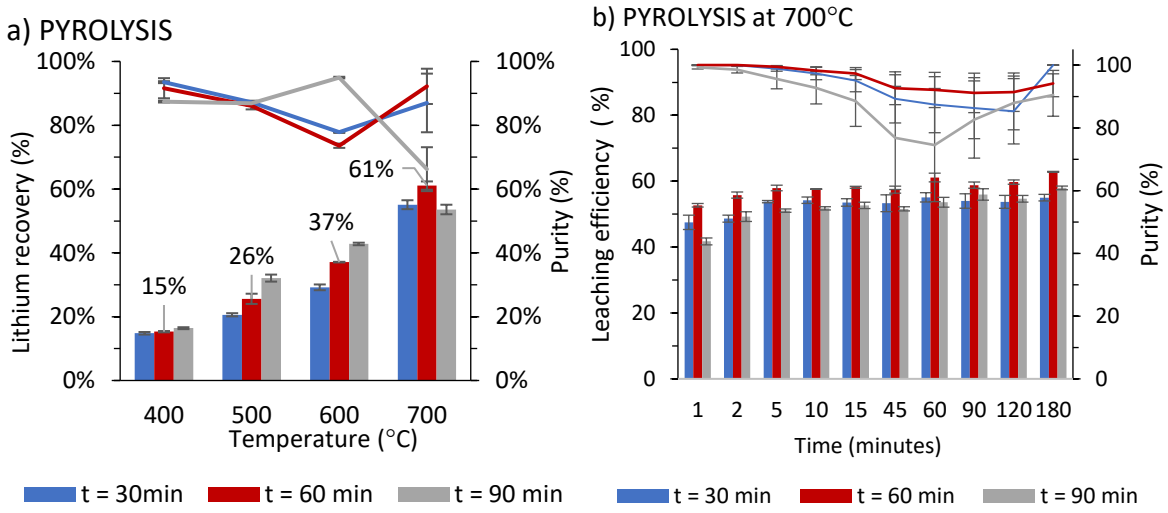

Figure 9: a) Lithium recovery (Left axis – histogram) and purity (Right axis) after pyrolysis at different temperatures (400–700°C) and treatment time (30–90 min) followed by water leaching (S/L = 20 g/L, 25°C, 1 h, 300 rpm) and b) after pyrolysis at 700°C for 3 different treatment times and water leaching at 25°C, S/L = 20 g/L

The optimal conditions are as follows: a treatment time of 1 h at 700°C, which resulted in a recovery of 61% and a purity of 92%. Under these conditions, the concentration of lithium and aluminium in the leachate was 370 mg/L and about 50 mg/L, respectively. Taking into consideration that under this condition, all oxides are determined to be reduced and that the total lithium recovery is not reached, it indicates that lithium is present in non-water-soluble species. The most expected one is lithium fluoride. However, some authors reported $LiAlO_2$ product of the reduction of the lithium metal oxide with the aluminium. $LiAlO_2$ is a stable oxide reported insoluble in water [51]. At high temperatures, aluminium can actually act as a reductant (Equation 31). This exothermic reaction is spontaneous, with a ΔG of -511.8 kJ at 600°C.

$$Al + \ LiCoO_{2,s} \rightarrow \ LiAlO_{2,s} + Co \quad (31)$$

However, both species (LiF and $LiAlO_2$) are very hard to identify in the sample by means of the analytical methods used, since they are under the device's limit of detection.

Kinetics studies were performed for the most promising temperature (700°C) for both incineration and pyrolysis at 3 different treatment times (Figure 9b). The recovery rate of lithium in water reaches an equilibrium after 20 minutes of leaching and there are no water-soluble forms of lithium remaining in the solid phase after this time at 25°C. For aluminium, the leaching yield

increases as the contact time increases, although its dissolution kinetics is slower than that of lithium. This is an important observation as it could lead to more selective leaching by shortening the contact time and thus avoiding the extraction of aluminium.

6.1.4 Solid residue composition

After evaporative crystallization of the leachate, the solid sample was analysed using XRD to identify the different salts present in the sample and the elemental composition was determined by ICP. Both aluminium and lithium were detected in the residue, with a lithium purity of 92% (after pyrolysis at 700˚C for 60 min). The diffraction patterns for four samples are shown in Figure 10 (incineration and pyrolysis at 600˚C and 700˚C for 60 min). These patterns were compared to the database (ICDD) for two different lithium salts (lithium carbonate and fluoride), indicating the presence of lithium carbonate. The additional peaks were assigned to lithium fluoride. The presence of aluminium was not detected using the XRD, which can be explained by the very small amount of aluminium in the residue (0.5 to 2.5 w%) which is under the detection limit for XRD.

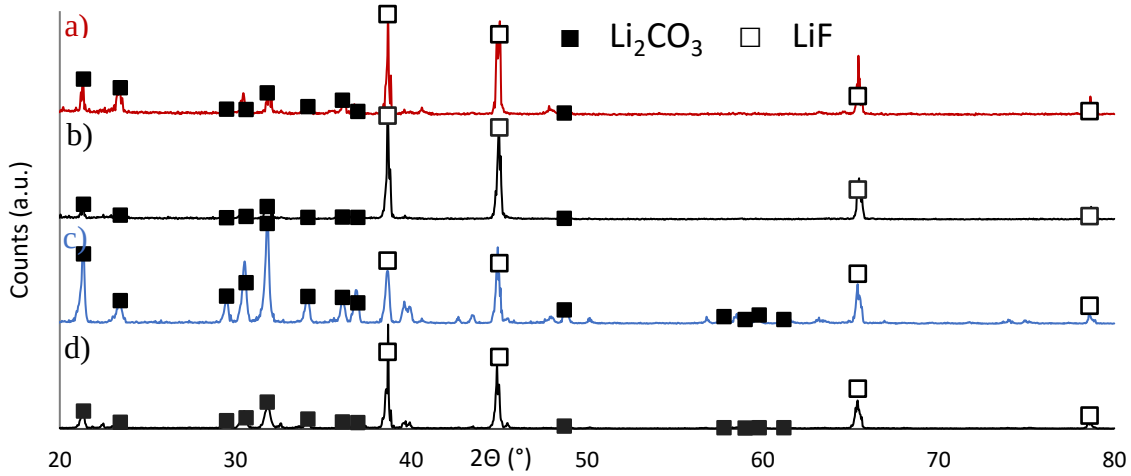

Figure 10: XRD pattern of residue obtained after evaporative crystallization of the leachate. The leaching (25 °C, S/L = 20 g/L for 60 min) was realized on different treated materials obtained after a) Incineration at 700°C for 60 minutes, b) Incineration at 600°C for 60 minutes, c) Pyrolysis at 700°C for 60 minutes and d) Pyrolysis at 600°C for 60 minutes.

The formation of lithium fluoride can be explained by the presence of fluorine in the leachate solution, which would react with lithium ions coming from the dissolution of lithium carbonate. The fluoride content was measured by an ion-selective electrode to quantify the amount of lithium fluoride. After pyrolysis at 700˚C for 60 minutes, there is about 1 mmol of fluoride per gram solid, which represents 2.3% of lithium fluoride formation against 97.7% of lithium carbonate.

This research work has brought clarity regarding the conditions needed for a high lithium recovery after thermal treatment and water leaching:

1) The separator has a significant positive effect on the lithium carbonate formation. This has not been demonstrated before and constitutes one of the major findings of the work.
2) Pyrolysis is favoured for carbothermic reduction. More carbon is available for the formation of the carbonates since carbon is not oxidized by the oxygen from the air.
3) The production of certain lithium compounds, such as LiF and $LiAlO_2$, limit its leachability with water.
4) The formation of lithium fluoride in the residue is problematic, and the conditions promoting its formation have not been determined.

6.2 Approach 2

6.2.1 Characterization of the solid sample

The elemental composition of each fraction obtained after sieving can be seen in Table 8. The fine fraction presented a much smaller content of aluminium and copper.

Table 8: Elemental composition (wt%) of different fractions from the black mass (*****indicates that the fractions were used in the subsequent experiments). Averages and standard deviation for triplicates.

Fraction / Element	Co	Ni	Mn	Li	Cu	Al	Fe	Total wt%
Black Mass wt%	10.5 ± 0.3	8.2 ± 0.2	7.5 ± 0.1	3.4 ± 0.1	7.8 ± 0.1	3.5 ± 0.1	0.2± 0.1	100
BM +500 µm wt%	5.3 ± 0.2	4.6 ± 0.1	4.3 ± 0.1	1.8 ± 0.1	19.0 ± 2.0	8.5 ± 0.9	0.1± 0.1	31
BM -500 µm wt%*	10.8 ± 0.4	8.6 ± 0.3	8.0 ± 0.3	3.3 ± 0.1	4.3 ± 0.3	1.1 ± 0.1	0.1± 0.1	69

6.2.2 Factorial design of experiments and regression models

The experimental conditions tested in the factorial design of experiments and the correspondent responses as leching efficiency for different metals are presented in Table 9. The fitted regression models for each metal and the coefficients of determination (R^2) are found in Table 10 (Equations 32–37). It is important to highlight that the models are valid within the range set in the experimental design and that only statistically significant terms are represented in each model (*p*-value < 0.05). Tests 9 to 12 correspond to the replicates in the central level of design, which allow estimation of the pure error, enabling the calculation of the lack of fit once the residuals are calculated. No experimental error could be determined for aluminium given its complete dissolution (leaching yield of 100%) in all the replicates in the central point.

Table 9: Experimental design and correspondent responses expressed as leaching efficiency of different metals.

Tests (Std Order)	Coded variables			Real variables			Responses (Y) - Leaching yield (%)					
	x1	x2	x3	OA concentration (M)	Time (min)	Temp (°C)	Li	Al	Mn	Co	Ni	Cu
1	-1	-1	-1	0.3	15	35	39.6	41.7	5.1	1.0	3.0	4.0
2	1	-1	-1	0.9	15	35	43.2	42.2	6.3	1.0	3.0	2.9
3	-1	1	-1	0.3	105	35	71.1	90.4	4.0	1.1	2.5	5.4
4	1	1	-1	0.9	105	35	87.2	90.7	4.2	0.5	0.5	0.4
5	-1	-1	1	0.3	15	65	77.6	78.7	4.6	2.2	3.9	5.2
6	1	-1	1	0.9	15	65	91.1	93.0	4.9	0.5	0.4	1.0
7	-1	1	1	0.3	105	65	80.9	100.0	3.8	1.6	1.4	4.2
8	1	1	1	0.9	105	65	96.1	100.0	5.5	0.5	0.0	4.6
9	0	0	0	0.6	60	50	91.8	100.0	2.4	0.4	0.2	0.9
10	0	0	0	0.6	60	50	91.7	100.0	2.3	0.5	0.5	1.0
11	0	0	0	0.6	60	50	93.2	100.0	2.3	0.4	0.3	1.0
12	0	0	0	0.6	60	50	91.1	100.0	2.5	0.4	0.3	0.8
13	-1	0	0	0.3	60	50	76.3	75.6	4.4	1.9	3.5	7.3
14	1	0	0	0.9	60	50	95.6	100.0	3.9	0.5	0.3	0.6
15	0	-1	0	0.6	15	50	74.9	58.7	4.4	0.7	1.2	0.5
16	0	1	0	0.6	105	50	97.9	95.6	2.2	0.4	0.0	2.4
17	0	0	-1	0.6	60	35	74.9	70.7	4.3	0.5	0.8	0.4
18	0	0	1	0.6	60	65	96.6	100.0	2.7	0.5	0.0	3.4

Table 10: Regression models for leaching yield of each element with their respective R^2.

Equations	R^2	
$\boldsymbol{Li}\ (\%) = \mathbf{92.09 + 6.76x_1 + 10.68x_2 + 12.61x_3 - 8.40x_2x_3 - 6.33x_1^2 - 5.85x_2^2 - 6.50x_3^2}$	0.99	(32)
$\boldsymbol{Al}\ (\%) = \mathbf{94.43 + 16.24x_2 + 13.58x_3 - 8.60x_2x_3}$	0.92	(33)
$\boldsymbol{Mn}\ (\%) = \mathbf{2.64 - 0.55x_2 + 1.22x_1^2}$	0.88	(34)
$\boldsymbol{Cu}\ (\%) = \mathbf{1.32\ - 1.66x_1 + 2.28\ x_1^2}$	0.85	(35)
$\boldsymbol{Co}\ (\%) = \mathbf{0.48 - 0.48x_1 - 0.29x_1x_3 + 0.16x_1x_2x_3 + 0.63x_1^2}$	0.96	(36)
$\boldsymbol{Ni}\ (\%) = \mathbf{0.40 - 1.01\ x_1 - 0.70x_2 - 0.41x_3 - 0.37x_1x_3 + 0.52x_1x_2x_3 + 1.41x_1^2}$	0.96	(37)

The results for the analysis of variance of the fitted model for lithium extraction are presented in Table 11. The significance of the regression model can be evaluated based on the F-value. Moreover, a Lack of Fit test was used to assess the model adequacy, but the value is slightly below the significant level of 0.0441. In this case, the variance of the residual error is higher than the estimated variance for the experimental error. This is not surprising considering the very small variation observed in the central point; thus, the experimental error is very low.

Table 11: Results for the analysis of variance of the fitted model for lithium extraction.

ELEMENT	SOURCE	DEGREES OF FREEDOM	SUM OF SQUARE (SS)	MEAN SQUARE (MS)	F-VALUE	p-VALUE
Lithium	Total	17	4922.4	289.6	-	-
	Regression	10	4889.1	488.9	102.8	0.000001
	Residual	7	33.3	4.8	-	-
	Lack of Fit	4	31.0	7.7	10.0	0.0441
	Pure error	3	2.3	0.8	-	-

The plot representing the observed response vs. the predicted response by the fitted model for lithium extraction is presented in Figure 11. The goodness-of-fit of the model is demonstrated in Figure 11. The higher the coefficient of determination, R^2, the better the model fits the experimental data. Here, the R^2 is very high (99%), which indicates that the fitted model can describe the variability in the data well.

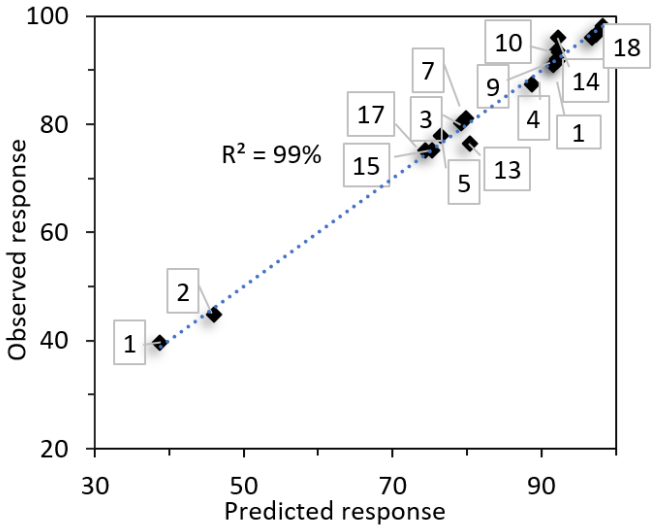

Figure 11: Plot representing the observed response vs. the predicted response by the fitted model for lithium extraction for each test number.

The standardized effects of the evaluated variables were plotted using Excel software and are represented as horizontal bars in the Pareto chart shown in Figure 12a. The red dashed line indicates the significance level (*p*-value < 0.05). The standardized effects of highly significant variables are located further to the right of the dashed line. Time and temperature are the variables with the main significant effect on lithium dissolution. No three-way interaction ($x_1x_2x_3$) or second-order acid concentration term (x_1x_2 and x_1x_3) were included in the reduced regression model. Moreover, the normal probability plot in Figure 12b is close to a straight line (R^2 = 98%), indicating that the residual distribution is approximately normal. Figure 12c shows that the residual seems to be generally random, confirming the independence of the errors and the absence of correlation. No real pattern can be observed in Figure 12d, which shows that the residuals are structureless and unrelated to the response. Thus, the residuals are randomly distributed, and the modelling errors are normally and independently distributed.

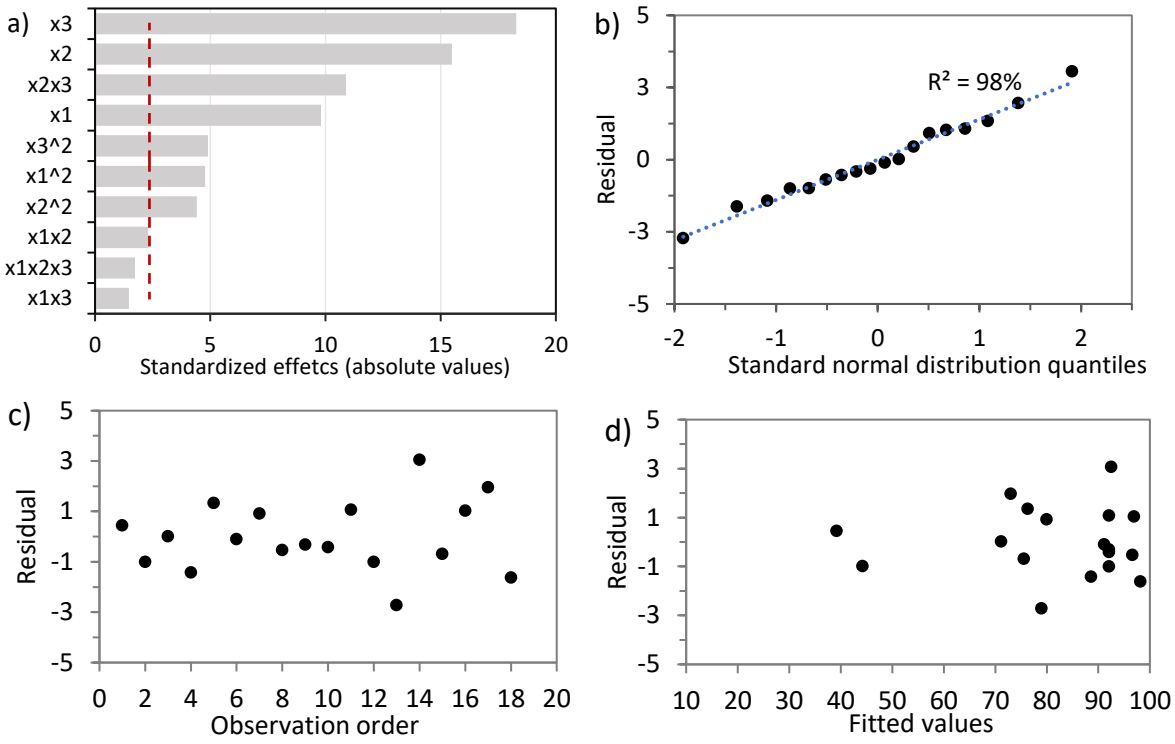

Figure 12: Pareto chart of the standardized effects of the factors (x_1: acid concentration, x_2: time, and x_3: temperature) for the regression model of Lithium (a) and Analysis of residuals: standard normal distribution of the residuals (b), residual versus observation order (c), residuals versus fitted values (d), and Response predicted by the model versus experimentally observed response (e).

The general observation which can made from the analysis of Table 9 is that the leaching yield is very high for lithium and aluminium (almost completely leached in certain conditions), while it is very low for the rest of the transition metals. Contour plots will be used to better visualize the leaching behaviour of lithium and select the parameters allowing better dissolution.

6.2.3 Response surface and contour plots

The response surfaces and contour plots for each element were plotted using Equations 32–37. This method helps to highlight the relations existing between the different variables of the operation. The contour plots display a two-dimensional view of the response surface, where all points that have the same response are connected to produce contour lines of constant responses. In a surface plot, the response surface is viewed as a three-dimensional surface.

The surface plots of lithium leaching yield are shown in Figure 13, including yields between 50 and 100%. It is important to stress that its dissolution is influenced by all the factors investigated in this study. The oxalic acid concentration, time, and temperature have a positive effect on lithium dissolution. At the low level of each parameter, the yield is only around 50%, and it reaches more than 90% at the central level of the design. Considering the goal of reaching the complete dissolution of lithium with milder conditions, it is already possible to target a different set of parameters that will allow an extraction over 95%. Those parameters are oxalic acid concentration of 0.6 M at 55°C for 60 minutes or oxalic acid concentration of 0.6 M at 40°C for 105 minutes. Below 0.45 M of oxalic acid, less than 90% of the lithium is extracted.

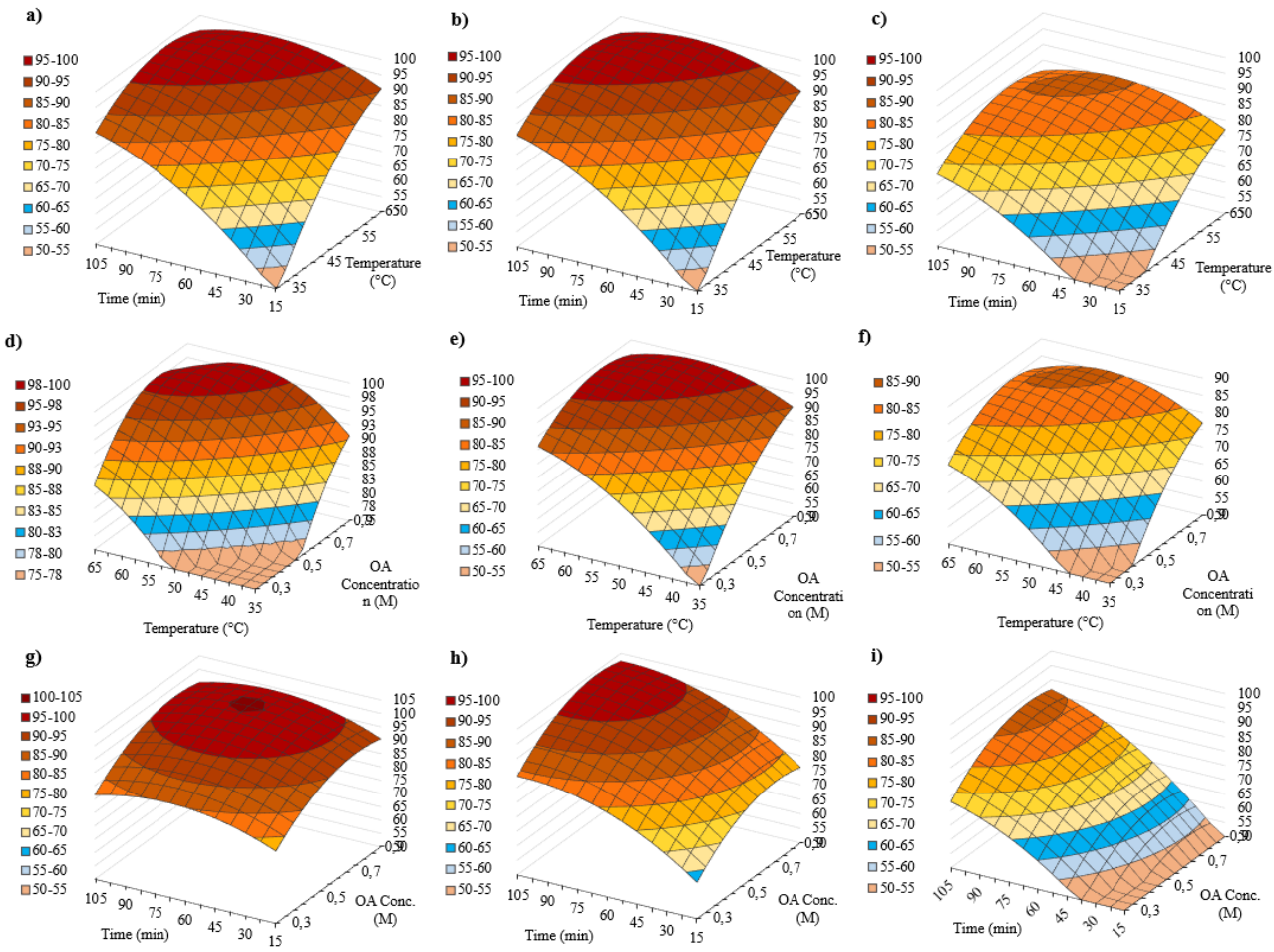

Figure 13: Lithium contour plots a) 0.9 M of oxalic acid, b) 0.6 M, c) 0.3 M, d) 105 min, e) 60 min, f) 15 min, g) 65°C, h) 50°C, and i) 35°C.

Aluminium dissolution is not influenced by the oxalic acid concentration as seen in Equation 33. One contour plot is relevant to observe the factors influencing the extraction as seen in Figure 14. It is shown that the dissolution increases with temperature and time from 50% of extraction in the smaller range of time and temperature (15 min and 35°C) to over 100% of extraction when the temperature goes over 60°C and leaching time is long. Complete extraction of aluminium was not expected and not reported by previous authors, who reported aluminium as a simple impurity without focusing on its leaching behaviour.

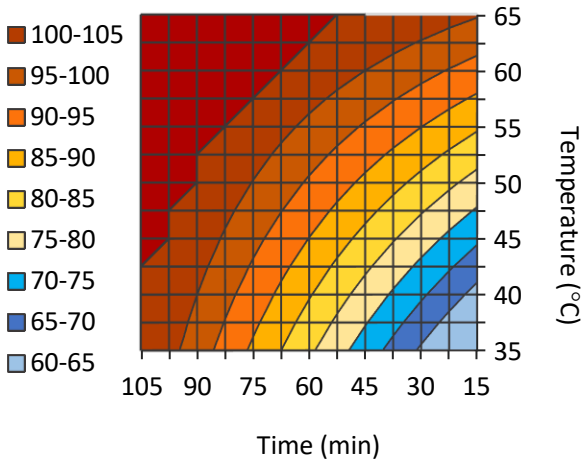

Figure 14: Aluminium leaching yield contour plots for oxalic acid concentration set at 0.3 – 0.6 – 0.9 M.

The behaviour of the other elements was also tracked (Figure 15), as predicted by Ka Ming et al. [40] Manganese is the element most extracted by oxalic acid due to the solubility of manganese oxalate. In this study, 2.4% of manganese was leached at the central point, which is lower than the dissolution previously observed by Ka Ming et al. [40] (around 20%). This can be explained by the dissolution time applied in their work, which was 12 hours. Since time has a positive effect on the dissolution of manganese, as seen in the regression model, Equation 34. Thus, if the reaction proceeds for a long time, there is a greater chance of the transition metals being found in the leachate if there is some oxalate available to react with. Nevertheless, the leachability of manganese is not considered problematic since it reached low yields, and manganese is not as valuable as the other transition metals. Moreover, it can be precipitated as $Mn(OH)_2$ when removing the aluminium from the leachate solution using sodium hydroxide. Equation 34 shows that the dissolution process of manganese is not influenced by temperature. At smaller concentrations of oxalic acid, final extraction decreased with time from about 4% to 0%. This highlights the two-step mechanism of the leaching. The first is the dissolution of the manganese as manganese oxalate and the second is its precipitation. On the other hand, higher concentration fosters higher leaching yield, up to 3.5%. This is because the insoluble oxalate can react with the oxalate excess present in the solution, forming soluble complexes.

When looking at the other transition metals, nickel, and cobalt dissolution remains lower than 1% with a decrease when temperature is increased. Moreover, time influences the dissolution. The longer the reaction is allowed to run, the great the number of elements that can be found as complex oxalate in the leachate. This correlates with the observation done on manganese dissolution. Finally, copper dissolution is influenced only by the oxalic acid concentration and a dissolution of about 1% was achieved using 0.6 M of oxalic acid.

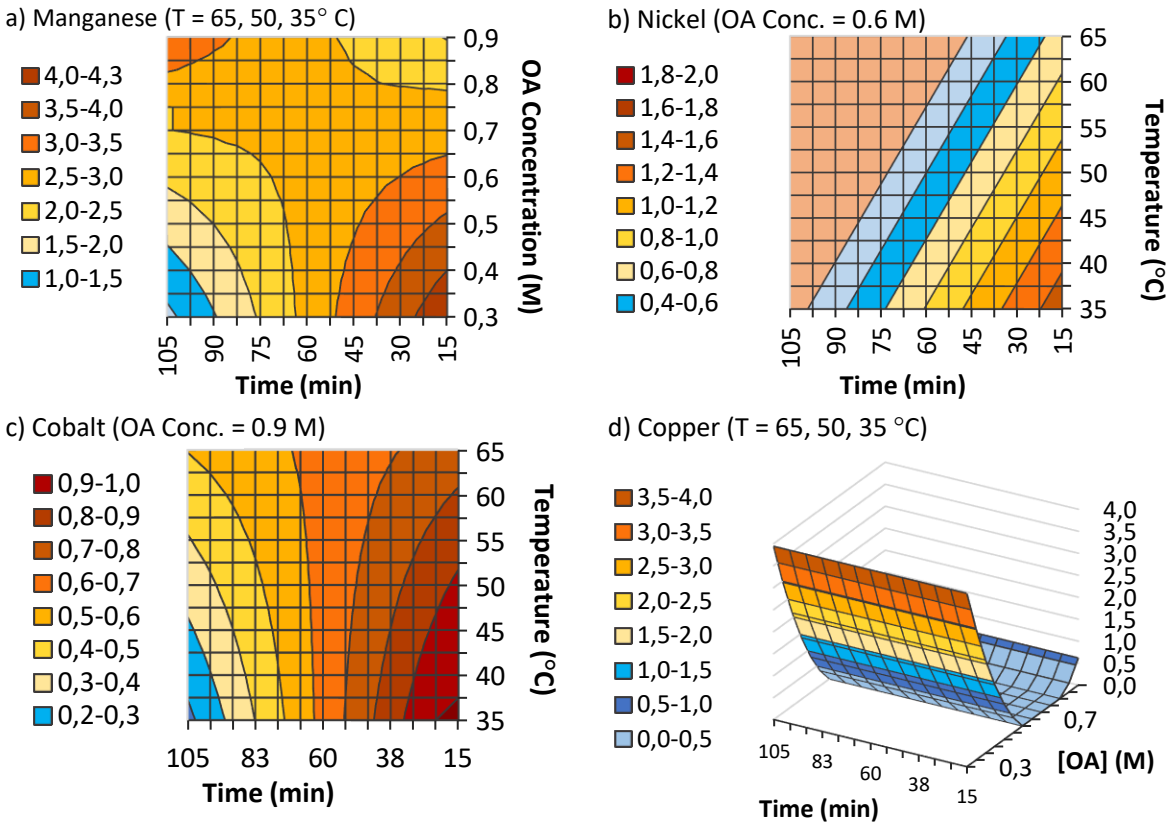

Figure 15: Contour plots representing leaching yield and modelled responses for manganese (a), nickel (b), cobalt (c), and copper (d).

After investigation of all the elements, the best set of parameters allowing the highest lithium yield, but the lowest dissolution of the transition metals, was identified. It corresponds to: temperature = 60°C, S/L = 50 g/L, oxalic acid concentration 0.6 M. These conditions were used in the upscaled experiments discussed in the next section to validate the regression models, as well as produce leaching residue to further investigate and confirm the leaching mechanism.

6.2.4 Upscaling the operation at optimal conditions

Validation of the fitted models

The leaching yields observed in the upscaled experiments under optimal conditions (temperature 60°C, S/L ratios 50 g/L, oxalic acid concentration 0.6 M) can be seen in Figure 16.

It is possible to observe that all the aluminium is leached in 30 minutes, which validates the observation made in the design of experiments and suggests the formation of aluminium oxalate complexes during the leaching operation. The total aluminium extraction does not represent a problem in the rest of the recycling process, since aluminium is normally removed before the separation of the transition metals. Having a leaching residue free of aluminium is convenient.

The leaching kinetics for lithium are very fast during the first 15 minutes, after which they slow down. 60 minutes were required to fully leach lithium. On the other hand, the dissolution of manganese, cobalt, and nickel decreases with time as they precipitate as oxalates. Copper

dissolution increased slightly after 60 minutes. Although this behaviour was not predicted by the model, which indicated independence from time, the final copper dissolution was very low (4.1%). The pH reaches a plateau after 60 minutes, increasing from 0.8 at the beginning of the reaction to 1.9. It is also important to highlight that the average concentration of lithium in the leachate is 1.7 g/L ± 0.1, compared with 0.60 g/L ± 0.01 g/L of aluminium (while 9 ppm of cobalt was detected and 37 ppm of copper).

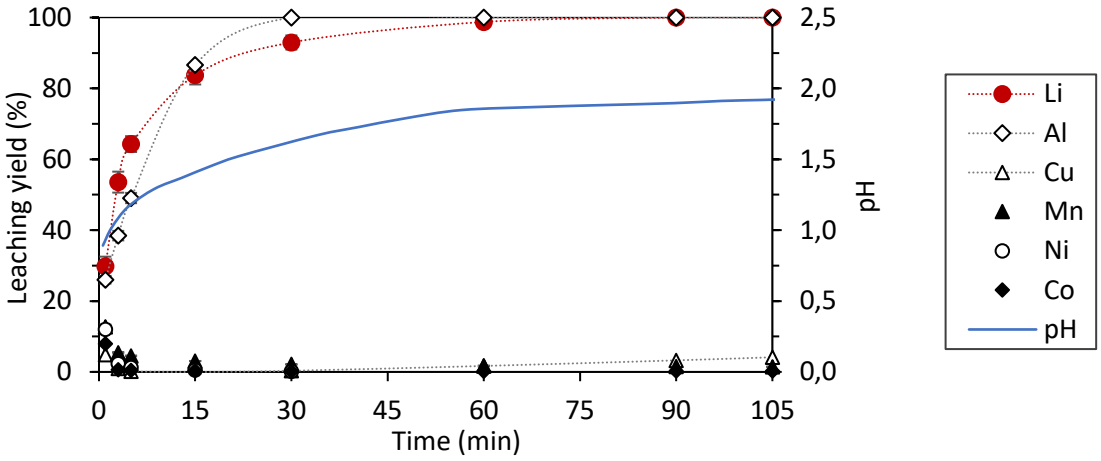

Figure 16: Leaching yields and pH evolution during the upscaled leaching experiment. Leaching conditions: temperature = 60°C, S/L = 50 g/L, oxalic acid concentration = 0.6 M.

A comparison of the predicted leaching yields calculated using Equations 32–37 with the obtained experimental values is presented in Table 12. It was confirmed that the fitted models are quite accurate when determining the leaching yield of lithium, aluminium, and copper, but had a higher deviation for nickel, cobalt, and manganese as very low extraction was observed for these metals. Moreover, it was observed that the selectivity of the operation is higher than predicted by the models, which is very promising for the future development of the process.

The leachate purification will be explored more deeply in future work. Different techniques can be considered, such as the precipitation of aluminium using sodium hydroxide. Lithium can then be recovered as lithium carbonate after precipitation with sodium carbonate, as performed in the work done by Ka Ming et al. [40].

Table 12: Leaching yield predicted (P) and experimental (E) with comparison of the STD of the experimental data (STD E) after 60 minutes, and the standard deviation (STD P/E) between the two values as well as the RSD P/E.

Element	Co	Ni	Mn	Li	Cu	Al
Yield P. (%)	0.48	0.18	2.64	97.7	1.32	100
Yield E. (%)	0.16	0.00	1.67	98.8	1.68	100
STD E. (%)	0.04	0.07	0.12	1.0	0.12	0
STD P/E. (%)	0.16	0.09	0.48	0.5	0.18	0
RSD P/E. (%)	100	-	29	1	11	-

Leaching residue characterization

The leaching residue was recovered after vacuum filtration and dried. The visual colour of the residue turned from dark black after sampling to a lighter grey colour. An increase in weight was observed, as the initial sample weight inserted in the leaching reactor was 3 g, and the residue recovered gained about 17% ± 3% weight. The elemental composition of the leaching residue is shown in Table 13 and the results validate the leaching calculated yields. No trace of aluminium was detected, confirming its total dissolution, while only 0.4% of residual lithium was detected. This constitutes an important finding of this work since no other authors observed a leaching of aluminium as high as shown in this work. There is a decrease in the elemental composition of other elements (nickel, cobalt, manganese, and copper) in the residue when compared to the initial sample, but this gap is explained by the residue's gain in mass due to the oxalate formation.

Table 13: Elemental analysis of the leaching residue in %wt (* remind the feed material).

Element / Fraction	Co	Ni	Mn	Li	Cu	Al	Fe
BM -500 µm wt% *	10.8 ± 0.4	8.6 ± 0.3	8.0 ± 0.3	3.3 ± 0.1	4.3 ± 0.3	1.1 ± 0.1	0.1± 0.1
Leaching residue wt%	8.0 ± 0.1	7.1 ± 0.1	6.1 ± 0.1	0.4 ± 0.0	2.9 ± 0.1	0.0 ± 0.0	/

The XRD pattern determined the nickel, cobalt, and manganese oxalates in the residue as seen in Figure 17. Copper and graphite remain in the residue as they did not react with oxalic acid. However, there is no evidence of remaining cathode-active material in the form of NMC 111 in the residue as observed by Renjie Chen et al. [39]. This difference can be explained by the analytical method applied. Assuming all the lithium remaining in the residue is some unreacted NMC cathode material and considering the very small amount of lithium (0.4%), the detection of NMC material by XRD is compromised under its detection limit.

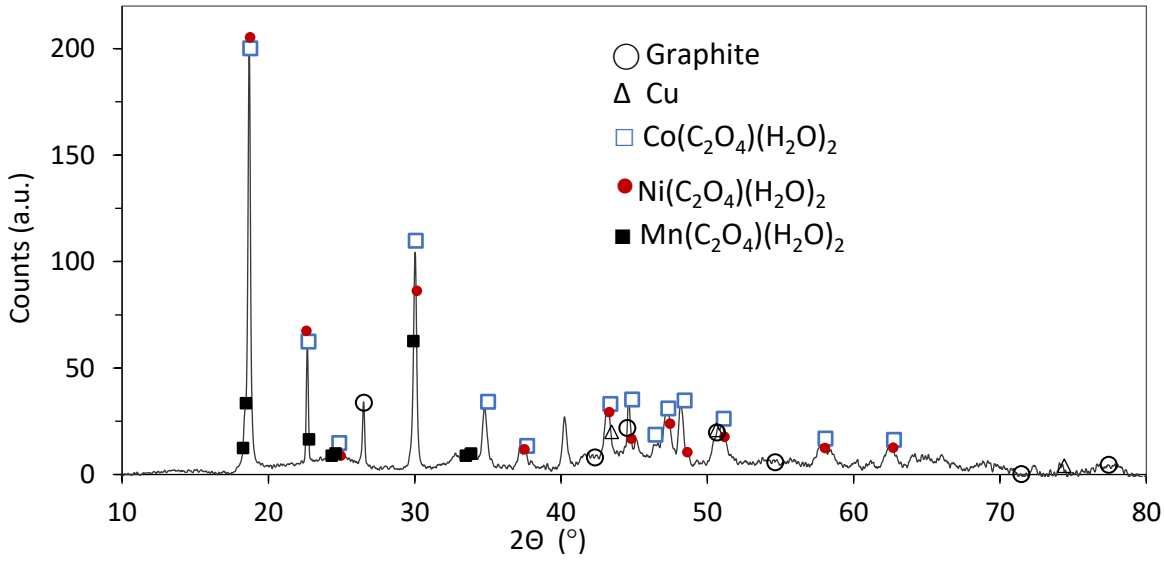

Figure 17: XRD pattern of the leaching residue; Graphite PDF 04-013-0292, Cu PDF 04-009-2090, Co(C2O4)(H2O)2 PDF 04-016-6937, Ni(C2O4)(H2O)2 PDF 04-016-6938, Mn(C2O4)(H2O)2 PDF 01-086-6854.

The FT-IR spectra in Figure 18 reveals five main peaks. The first peak at 3373.5 cm^{-1} is attributed to the residual hydration of the oxalates compound (O-H stretching vibration). The peak at 1622 cm^{-1} is assigned to the asymmetric O-C-O of the carboxyl group, while the peaks at 1359.5 and 1314.5 cm^{-1} are associated with the symmetric of the same carboxyl function. Thus, the FT-IR measurement correlates with the XRD analysis showing the precipitation of nickel, cobalt, and manganese oxalate, and these findings were also verified in the work of Qui K. et al [46].

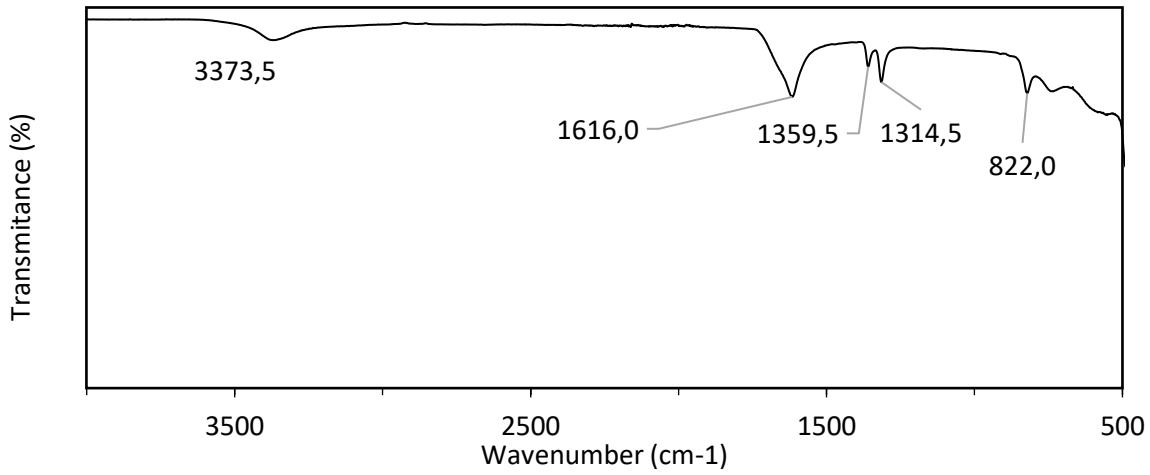

Figure 18: FT-IR analysis of the leaching residue.

This work leads to some conclusive statements about the selective leaching of lithium using oxalic acid:

1) The design of experiments allows the determination of the optimal factors influencing the reaction.
2) 98% of the lithium is recovered in the leachate and 100 % of the aluminium is co-dissolved, a new finding not previously reported in the literature.
3) Less than 0.5 % of the cobalt and nickel is dissolved and about 1.5 % of the manganese is co-leached.

7 Summary and conclusions

The main scope of this work was to improve the total lithium recovery from LiB. Two approaches were investigated: a thermal treatment followed by water leaching and oxalic acid leaching without prior thermal treatment. Evaluation of the operation is mainly via the leaching yield of lithium but the behaviour of each of the other metals was also followed along the process. It was shown that the lithium recovery could be significantly increase.

In the first approach, the main outcomes of the study are the following:

1) The separator is proven to have a positive effect on lithium recovery, acting as a source of carbon for the formation of lithium carbonate in the furnace between 500°C and 700°C.
2) Pyrolysis is evaluated as being the most promising treatment, with increasing treatment temperature and time having a positive effect on the subsequent leaching yield of lithium.
3) A maximal lithium recovery of 62% was obtained after pyrolysis at 700°C for 60 min and water leaching at 25°C with a S/L of 20 g/L. The limitation on the recovery is evaluated as the presence of alternative lithium compounds which are not water soluble, such as LiF or $LiAlO_2$.
4) A lithium purity of 92% was measured in the leachate. The only impurity co-extracted with lithium is aluminium, with extraction increasing with temperature and time. The hypothesis is that aluminium fluoride is formed, which can be leached with water.
5) The characterization of the crystal residue shows the presence of aluminium and lithium, with the same purity as in the leachate. XRD analysis proves the mix of lithium carbonate and lithium fluoride (aluminium is not detected due to the detection limit), an estimated 2.3% of lithium fluoride is present in the residue.

In the second approach, regression models representing the leaching yield of lithium, aluminium, copper, cobalt, manganese, and nickel were validated and contour plots helped to analyse the dissolution process. The main outcomes of this work are the following:

1) A minimum of 0.45 M of oxalic acid is required to reach a lithium dissolution of over 90% at S/L ratios of 50g/L.
2) Aluminium is entirely leached under most of the tested conditions, which is a novel finding of this study since this behaviour has never been reported by other authors as being so complete.
3) High leaching selectivity was achieved for lithium versus the other metals, which presented very low dissolution. From the transition metals, manganese was the one more extracted, with only 2.4% leaching yield in the central point of the design.
4) The optimum parameters identified in this work are 60°C, 60 minutes, and 0.6 M of oxalic acid at the fixed S/L of 50g/L. The final leaching yields are: 98.8% of the lithium and 100% of aluminium were leached, while less than 0.5 % of cobalt and nickel, and 1.5% of manganese were dissolved.
5) Leaching residue analysis confirm the presence of the carboxyl group in the residue (with FT-IR analysis), while the presence of cobalt, manganese, and nickel oxalates formed and precipitated during the leaching was confirmed by XRD.

8 Future work

In the first approach, the preliminary work has allowed the identification of different problems. First, HF formation is an issue as it reacts with lithium and aluminium to form lithium fluoride and aluminium fluoride. Moreover, the fluoride dissolves in water, which can then react with lithium-ion in solution and form lithium fluoride during evaporative crystallization. Thus, the purity of lithium carbonate produced is affected. The first working angle will be the neutralization of the HF directly in the furnace. Some addition of calcium carbonate in the black mass mixture will be considered. Secondly, the co-extraction of aluminium needs to be minimized. As explained in the thesis, decreasing the leaching time seems to be beneficial to decrease aluminium dissolution. If this is not sufficient, aluminium precipitation can be performed using sodium hydroxide on the leachate. Finally, a limitation in the transformation of lithium into lithium carbonate has been observed. The water alone cannot leach all lithium compounds. The addition of alkaline in the leaching agent will be examined.

A very efficient way to achieve early selective lithium recovery from spent lithium-ion batteries was demonstrated in the second approach. To develop and estimate the full feasibility of the process at an industrial level, some additional studies will be performed. The first one will be to investigate the leachability of the NMC oxalates left in residue, and then their purification. The purification of the leachate solution containing mainly aluminium, plus lithium will then be studied; aluminium removal by means of sodium hydroxide precipitation will be considered and solvent extraction or ion exchange for lithium recovery will be investigated.

Acknowledgments

This work was possible thanks to the Swedish Energy Agency – Battery fund (Grants No: 52009-1) and BASE (Batteries Sweden) by Vinnova (Grant No. 2019-00064). The authors would like to acknowledge the support of Volvo Cars AB. Stena Recycling International AB, and Akkuser Oy for providing samples and for valuable discussions.

I would like to thank my supervisor Martina Petranikova for her trust, support and help during these last two years. To my ex-co-supervisor, Nathália Vieceli, thank you very much for your help in the lab and outside, listening to my problems and helping me carrying out with new project. I am also grateful to Burcak Ebin, my co-supervisor, for your feedback, guidance and support in the last past months. Thank you to my examiner Teodora Retegan Vollmer for helping me get started and for being part of my education.

Thanks to all my friends Nils, Thomas, Luis, Dogac, and Ioanna and colleagues in NC/IMR for making this a fun and wonderful journey.

I am extremely grateful to my family and friends; you have been following me for the last years with a lot of love and support. My last work will be for you, Alejandro, thank you for being the best partner I ever wished for, we form the best team, and I am looking forward to seeing all new adventures life is having for us.

Bibliography

1. IEA, P. Electric Vehicles - Technology Deep Drive - Tracking Report Available online: https://www.iea.org/reports/electric-vehicles, License: CC BY 4.0 (accessed on 19 January 2023).

2. International Energy Agency (IEA) Global EV Outlook 2021 - Accelerating Ambitions despite the Pandemic. *Global EV Outlook 2021* **2021**.

3. Energy Agency, I. Global EV Outlook 2022 Securing Supplies for an Electric Future. **2022**.

4. European parliament Deal Confirms Zero-Emissions Target for New Cars and Vans in 2035 Available online: https://www.europarl.europa.eu/news/en/press-room/20221024IPR45734/deal-confirms-zero-emissions-target-for-new-cars-and-vans-in-2035 (accessed on 19 January 2023).

5. Scrosati, B.; Garche, J. Lithium Batteries: Status, Prospects and Future. *J Power Sources* **2010**, *195*, 2419–2430, doi:10.1016/j.jpowsour.2009.11.048.

6. Armand, M.; Axmann, P.; Bresser, D.; Copley, M.; Edstr, K.; Ekberg, C.; Guyomard, D.; Lestriez, B.; Nov, P.; Petranikova, M.; et al. Lithium-Ion Batteries – Current State of the Art and Anticipated Developments. *Power sources* **2020**, *479*, 26, doi:10.1016/j.jpowsour.2020.228708.

7. Larouche, F.; Tedjar, F.; Amouzegar, K.; Houlachi, G.; Bouchard, P.; Demopoulos, G.P.; Zaghib, K. Progress and Status of Hydrometallurgical and Direct Recycling of Li-Ion Batteries and Beyond. *Materials* **2020**, *13*, doi:10.3390/ma13030801.

8. U.S. Geological Survey (USGS) Lithium Data - Mineral Commodity Summaries. **2018**, 2017–2018.

9. U.S Geological Survey Lithium Data - Mineral Commodity Summary. *U.S Geological Survey* **2022**, 2021–2022.

10. Kesler, S.E.; Gruber, P.W.; Medina, P.A.; Keoleian, G.A.; Everson, M.P.; Wallington, T.J. Global Lithium Resources: Relative Importance of Pegmatite, Brine and Other Deposits. *Ore Geol Rev* **2012**, *48*, 55–69, doi:10.1016/j.oregeorev.2012.05.006.

11. Christmann, P.; Gloaguen, E.; Labbé, J.F.; Melleton, J.; Piantone, P. Chap1 : Global Lithium Resources and Sustainability Issues. In *Lithium Process Chemistry: Resources, Extraction, Batteries, and Recycling*; Elsevier Inc., 2015; pp. 1–40 ISBN 9780128014172.

12. European Comission RMIS – Raw Materials Profiles - Lithium Available online: https://rmis.jrc.ec.europa.eu/apps/rmp2/#/Lithium (accessed on 20 February 2023).

13. European commission *Critical Raw Materials Resilience: Charting a Path towards Greater Security and Sustainability*; 2020;

14. European commission *REGULATION OF THE EUROPEAN PARLIAMENT AND OF THE COUNCIL Concerning Batteries and Waste Batteries*; 2020; Vol. 353;.

15. Dewulf, J.; Van der Vorst, G.; Denturck, K.; Van Langenhove, H.; Ghyoot, W.; Tytgat, J.; Vandeputte, K. Recycling Rechargeable Lithium Ion Batteries: Critical Analysis of Natural Resource Savings. *Resour Conserv Recycl* **2010**, *54*, 229–234, doi:10.1016/j.resconrec.2009.08.004.

16. Christian Julien, Alain Mauger, Ashok Vijh, K.Z. *Lithium Batteries Science and Technology*; 2016; Vol. 15; ISBN 9783319191072.

17. Nunes-Pereira, J.; Costa, C.M.; Lanceros-Méndez, S. Polymer Composites and Blends for Battery Separators: State of the Art, Challenges and Future Trends. *J Power Sources* **2015**, *281*, 378–398, doi:10.1016/j.jpowsour.2015.02.010.

18. Neumann, J.; Petranikova, M.; Meeus, M.; Gamarra, J.D.; Younesi, R.; Winter, M.; Nowak, S. Recycling of Lithium-Ion Batteries—Current State of the Art, Circular Economy, and Next Generation Recycling. *Adv Energy Mater* **2022**, *2102917*, doi:10.1002/aenm.202102917.

19. Winslow, K.M.; Laux, S.J.; Townsend, T.G. A Review on the Growing Concern and Potential Management Strategies of Waste Lithium-Ion Batteries. *Resour Conserv Recycl* **2018**, *129*, 263–277, doi:10.1016/j.resconrec.2017.11.001.

20. Gerold, E.; Schinnerl, C.; Antrekowitsch, H. Critical Evaluation of the Potential of Organic Acids for the Environmentally Friendly Recycling of Spent Lithium-Ion Batteries. *Recycling* **2022**, *7*, 4.

21. Lombardo, G. Comparison of Incineration and Pyrolysis of NMC-Lithium-Ion Batteries – Determination of the Effects on the Chemical Composition , and Potential Formation of Hazardous by-Products . PhD Thesis, Chalmers University of Technology, 2020.

22. Jung, J.; Sui, P.-C.; Zhang, J. *Hydrometallurgical Recycling of Lithium-Ion Battery Materials*; 2023; ISBN 9781032216027.

23. Hampel, C. *Electrive.com*. 2022,.

24. MAISCH, M. *PV magazine*. 2019,.

25. Brian Makuza, Qinghua Tian, Xueyi Guo, Kinnor Chattopadhyay, D.Y. Pyrometallurgical Options for Recycling Spent Lithium-Ion Batteries_ A Comprehensive Review. *Power sources* **2021**, *491*.

26. Petranikova, M.; Naharro, P.L.; Vieceli, N.; Lombardo, G.; Ebin, B. Recovery of Critical Metals from EV Batteries via Thermal Treatment and Leaching with Sulphuric Acid at

Ambient Temperature. *Waste Management* **2022**, *140*, 164–172, doi:10.1016/j.wasman.2021.11.030.

27. Lim, F.-P. 'Black Mass' Needs Common Global Specs to Commoditize Recycled Battery Raw Materials Available online: https://www.fastmarkets.com/insights/black-mass-needs-common-global-specs-to-commoditize-recycled-battery-raw-materials (accessed on 22 March 2023).

28. Umicore Our Recycling Process Available online: https://csm.umicore.com/en/battery-recycling/our-recycling-process/ (accessed on 21 July 2021).

29. Harper, G.; Anderson, P.A.; Kendrick, E.; Mrozik, W.; Christensen, P.; Lambert, S.; Greenwood, D.; Das, P.K.; Ahmeid, M.; Milojevic, Z.; et al. Roadmap for a Sustainable Circular Economy in Lithium-Ion and Future Battery Technologies. *Journal of Physics: Energy* **2022**, doi:10.1088/2515-7655/acaa57.

30. Umicore Our Recycling Process Available online: https://brs.umicore.com/en/recycling/ (accessed on 19 March 2023).

31. Golmohammadzadeh, R.; Faraji, F.; Rashchi, F. Recovery of Lithium and Cobalt from Spent Lithium Ion Batteries (LIBs) Using Organic Acids as Leaching Reagents : A Review. *Resour Conserv Recycl* **2018**, *136*, 418–435, doi:10.1016/j.resconrec.2018.04.024.

32. Xiao, J.; Li, J.; Xu, Z. Novel Approach for in Situ Recovery of Lithium Carbonate from Spent Lithium Ion Batteries Using Vacuum Metallurgy. *Environ Sci Technol* **2017**, *51*, 11960–11966, doi:10.1021/acs.est.7b02561.

33. Maroufi, S.; Assefi, M.; Khayyam Nekouei, R.; Sahajwalla, V. Recovery of Lithium and Cobalt from Waste Lithium-Ion Batteries through a Selective Isolation-Suspension Approach. *Sustainable Materials and Technologies* **2020**, *23*, 2–6, doi:10.1016/j.susmat.2019.e00139.

34. Jandová, J.; Dvořák, P.; Kondás, J.; Havlák, L. Recovery of Lithium from Waste Materials. *Ceramics - Silikaty* **2012**, *56*, 50–54.

35. Liu, P.; Xiao, L.; Tang, Y.; Chen, Y.; Ye, L.; Zhu, Y. Study on the Reduction Roasting of Spent LiNi x Co y Mn z O 2 Lithium-Ion Battery Cathode Materials. *J Therm Anal Calorim* **2019**, *136*, 1323–1332, doi:10.1007/s10973-018-7732-7.

36. Balachandran, S.; Forsberg, K.; Lemaître, T.; Lombardo, G.; Petranikova, M. Comparative Study for Selective Lithium Recovery via Chemical Transformations during Incineration and Dynamic Pyrolysis on EV Li-Ion Batteries. *Metals (Basel)* **2021**, *11*, 16.

37. Krishnamurty, K. v.; Harris, G.M.; Sastri, V.S. *The Chemistry of the Metal Carbonato Complexes*; 1960; Vol. 70;.

38. Sohn, J.S.; Shin, S.M.; Yang, D.H.; Kim, S.K.; Lee, C.K. Comparison of Two Acidic Leaching Processes for Selecting the Effective Recycle Process of Spent Lithium Ion Battery. *Geosystem Engineering* **2006**, *9*, 1–6, doi:10.1080/12269328.2006.10541246.

39. Zhang, X.; Bian, Y.; Xu, S.; Fan, E.; Xue, Q.; Guan, Y.; Wu, F.; Li, L.; Chen, R. Innovative Application of Acid Leaching to Regenerate Li(Ni1/3Co1/3Mn1/3)O2 Cathodes from Spent Lithium-Ion Batteries. *ACS Sustain Chem Eng* **2018**, *6*, 5959–5968, doi:10.1021/acssuschemeng.7b04373.

40. Li, Q.; Fung, K.Y.; Xu, L.; Wibowo, C.; Ng, K.M. Process Synthesis: Selective Recovery of Lithium from Lithium-Ion Battery Cathode Materials. *Ind Eng Chem Res* **2019**, *58*, 3118–3130, doi:10.1021/acs.iecr.8b04899.

41. Zeng, X.; Li, J.; Shen, B. Novel Approach to Recover Cobalt and Lithium from Spent Lithium-Ion Battery Using Oxalic Acid. *J Hazard Mater* **2015**, *295*, 112–118, doi:10.1016/j.jhazmat.2015.02.064.

42. Lombardo, G.; Ebin, B.; Mark, M.R.; Steenari, B.M.; Petranikova, M. Incineration of EV Lithium-Ion Batteries as a Pretreatment for Recycling – Determination of the Potential Formation of Hazardous by-Products and Effects on Metal Compounds. *J Hazard Mater* **2020**, *393*, 122372, doi:10.1016/j.jhazmat.2020.122372.

43. Kwon, O. sung; Sohn, I. Fundamental Thermokinetic Study of a Sustainable Lithium-Ion Battery Pyrometallurgical Recycling Process. *Resour Conserv Recycl* **2020**, *158*, 104809, doi:10.1016/j.resconrec.2020.104809.

44. M., M.; Hirschler Effect of Oxygen on the Thermal Decomposition of Poly(Vinylidene Fluoride). *Eur Polym J* **1982**, *18*, 463–467, doi:https://doi.org/10.1016/0014-3057(82)90184-7.

45. Schwich, L.; Schubert, T.; Friedrich, B. Early-Stage Recovery of Lithium from Tailored Thermal Conditioned Black Mass Part I : Mobilizing Lithium via Supercritical CO 2 - Carbonation. *Metals (Basel)* **2021**, *11*, 177.

46. Sun, L.; Qiu, K. Organic Oxalate as Leachant and Precipitant for the Recovery of Valuable Metals from Spent Lithium-Ion Batteries. *Waste Management* **2012**, *32*, 1575–1582, doi:10.1016/j.wasman.2012.03.027.

47. David R. Lide *CRC Handbook in Chemistry and Physics*; Standard R.;

48. Gerlach, R.W.; Dobb, D.E.; Raab, G.A.; Nocerino, J.M. Gy Sampling Theory in Environmental Studies. 1. Assessing Soil Splitting Protocols. *J Chemom* **2002**, *16*, 321–328, doi:10.1002/cem.705.

49. Douglas C. Montgomery *Design and Analysis of Experiments*; John Wiley & Sons, Ed.; 2009; ISBN 978-0-470-39882-1.

50. Lombardo, G.; Ebin, B.; St Foreman, M.R.J.; Steenari, B.M.; Petranikova, M. Chemical Transformations in Li-Ion Battery Electrode Materials by Carbothermic Reduction. *ACS Sustain Chem Eng* **2019**, *7*, 13668–13679, doi:10.1021/acssuschemeng.8b06540.

51. PubChem Lithium Aluminate Available online: https://pubchem.ncbi.nlm.nih.gov/compound/Lithium-aluminate#section=Experimental-Properties (accessed on 22 March 2023).